The Evolution of Whisker-Mediated Somatosensation in Mammals: Sensory Processing in Barrelless S1 Cortex of a Marsupial, *Monodelphis domestica*

Deepa L. Ramamurthy and Leah A. Krubitzer*

Center for Neuroscience, University of California, Davis, Davis, California 95618

ABSTRACT

Movable tactile sensors in the form of whiskers are present in most mammals, but sensory coding in the cortical whisker representation has been studied almost exclusively in mice and rats. Many species that possess whiskers lack the modular "barrel" organization found in the primary somatosensory cortex (S1) of mice and rats, but it is unclear how whisker-related input is represented in these species. We used single-unit extracellular recording techniques to characterize receptive fields and response properties in S1 of *Monodelphis domestica* (short-tailed opossum), a nocturnal, terrestrial marsupial that shared its last common ancestor with placental mammals over 160 million years ago. Short-tailed opossums lack barrels and septa in S1 but show active whisking behavior similar to that of mice and rats. Most neurons in short-tailed opossum S1 exhibited multiwhisker receptive fields, including a single best whisker (BW) and lower magnitude responses to the deflection of surrounding whiskers. Mean tuning width was similar to that reported for mice and rats. Both symmetrical and asymmetrical receptive fields were present. Neurons tuned to ventral whiskers tended to show broad tuning along the rostrocaudal axis. Thus, despite the absence of barrels, most receptive field properties were similar to those reported for mice and rats. However, unlike those species, S1 neuronal responses to BW and surround whisker deflection showed comparable latencies in short-tailed opossums. This dissimilarity suggests that some aspects of barrel cortex function may not generalize to tactile processing across mammalian species and may be related to differences in the architecture of the whisker-to-cortex pathway. J. Comp. Neurol. 524:3587–3613, 2016.

INDEXING TERMS: vibrissae; area 3b; receptive fields; barrels; touch; RRID:AB_477329

The emergence of body hair is one of the hallmarks that distinguishes mammals from all other extant vertebrate lineages. This evolutionary innovation allowed for the development of a novel class of movable tactile sensors in the form of sinus hairs, or whiskers (also referred to as *vibrissae*). Present-day mammals use their whiskers for a variety of behavioral functions, including the exploration of novel environments, object recognition, spatial navigation, prey capture, and social interactions (Anjum et. al, 2006; Brecht, 2007; Mitchinson et al., 2011; Feldmeyer et al., 2013; Bobrov et al., 2014; Sofroniew et al., 2014; Sofroniew and Svoboda, 2015). In fact, whiskers are known to be present at some point during development in nearly all taxa of marsupial and placental mammals (Pocock, 1914; Huber, 1930a,b; Lyne, 1958; Ahl, 1986; Sarko et al., 2011).

The prominent array of long facial whiskers present on the snout, known as the *mystacial whiskers*, is conserved across mammalian species and displays several species-invariant characteristics in its morphology, including a highly ordered, grid-like arrangement and a systematic variation in both whisker length and shape, depending on the position of a whisker within the array (Brecht et al., 1997; Towal et al., 2011). The pattern of innervation of the whisker follicles is similar in

Grant sponsor: National Eye Institute; Grant number: R01EY022987-01 (to L.A.K.); Grant number: 2T32EY015387-11 (to D.L.R.); Grant sponsor: National Science Foundation Graduate Research Fellowship Program; Grant number: DGE-1148897 (to D.L.R.).

*CORRESPONDENCE TO: Leah A. Krubitzer, Center for Neuroscience, University of California, Davis, 1544 Newton Court, Davis, CA 95618.
E-mail: lakrubitzer@ucdavis.edu

Received December 24, 2015; Revised April 13, 2016;
Accepted April 13, 2016.
DOI 10.1002/cne.24018
Published online May 10, 2016 in Wiley Online Library (wileyonlinelibrary.com)

marsupial and placental mammals (Patrizi and Munger, 1966; Lee and Woolsey, 1975; Welker and Van der Loos, 1986; Loo and Halata, 1991). In addition, marsupials and placentals share a common bauplan of facial musculature, which involves the muscles typically used to control whisker movement. This muscular arrangement is different from the organization of facial muscles in monotremes, which are highly derived and do not possess whiskers (Huber, 1930a,b; Grant et al., 2013). Whisker-mediated somatosensation was, therefore, likely present in the common ancestor of all marsupial and placental mammals and may have been especially important in exploration and object identification, given the nocturnal lifestyle of our early ancestors (Kemp, 2005; Heesy and Hall, 2010).

The whisker system is a major model for the study of several aspects of cortical function, including information encoding and processing, thalamocortical and corticocortical interactions, sensorimotor integration, and active touch sensing (Diamond et al., 2008; Fox and Woolsey, 2008; Feldmeyer et al., 2013; for review see Sofroniew and Svoboda, 2015). The discovery of cytoarchitecturally identifiable "barrels" in layer IV of the primary somatosensory cortex (S1), corresponding to the cortical map of the whiskers in mice (Woolsey and Van der Loos, 1970) and rats (Welker, 1971), combined with the availability of modern genetic and molecular techniques led to the establishment of barrel cortex as an ideal and widely used experimental system not only for the study of somatosensory processing but also for the study of neural circuit development, plasticity, and dysfunction.

There are currently over 5,500 extant species of mammals, distributed across 29 different orders, as recorded in the most recent taxonomic compilation of the known species of the world (Roskov et al., 2015). However, most of our knowledge with respect to the neural circuits that underlie cortical processing stems from the study of only a handful of model species. In particular, despite the ubiquity of whiskers in extant mammalian species, the entire body of research conducted on S1 barrel cortex has created a focus almost exclusively on mice and rats, two closely related genera from the family Muridae, which is just one of 29 families belonging to a single mammalian order, Rodentia (Roskov et al., 2015). As a result, there is an abundance of information on the structural and functional organization of S1 barrel cortex in the mouse and the rat, but little is known about which aspects of barrel cortex organization are derived features specific to murine rodents and which aspects can be generalized to the neural circuits involved in tactile processing across mammalian species. In the current investigation, we address this dearth of comparative studies on the organization of the whisker representation within the neocortex of mammals by examining the receptive fields and response characteristics of neurons in the S1 whisker representation of the short-tailed opossum *Monodelphis domestica*.

We chose to study this animal model for a number of reasons. First, this is a marsupial that shared its last common ancestor with placental mammals about 160 million years ago (Meredith et al., 2011; O'Leary et al., 2013). Studying the functional organization of S1 in short-tailed opossums could therefore provide important insights into the features of sensory processing circuits involved in whisker-mediated touch that are common to both marsupial and placental mammals. Second, the peripheral morphology of the whisker array in short-tailed opossums is similar to that in rats and mice (Brecht et al., 1997; Grant et al., 2013), which implies the existence of similar constraints as well as the use of comparable strategies in the sampling and coding of tactile information during whisker-mediated somatosensation. Third, similarly to mice and rats, these opossums exhibit a specialized behavior associated with the whiskers known as *whisking*, a stereotypic, rhythmic, back-and-forth movement of the facial whiskers during spatial exploration and navigation (Mitchinson et al., 2011; Grant et al., 2013). Whisking is not present in all animals that possess whiskers; this is an energetically expensive behavior that requires complex, specialized musculature (Huber, 1930a; Grant et al., 2013) and is hypothesized to provide a behavioral advantage by increasing the degrees of freedom available for positioning the tactile sensors (Grant et al., 2013).

Finally, there are known structural differences in S1 of short-tailed opossums compared with rats and mice. In rats, mice, and some other mammals, histological processing of S1 reveals the presence of a cell-dense modular cytoarchitecture consisting of the *barrels*, separated by cell-sparse regions called *septa* (Woolsey and

Abbreviations

3b	primary somatosensory cortex
A1	primary auditory cortex
BW	best whisker
CT	caudal temporal area
FBP	furry buccal pad
FM	frontal myelinated area
IM	intramuscular
IP	intraperitoneal
ISI	interspike interval
OB	olfactory bulb
PSTH	peristimulus time histogram
PV	parietal ventral area
PYR	piriform cortex
RF	receptive field
S1	primary somatosensory cortex
S2	secondary somatosensory cortex
SBW	second-best whisker
V1	primary visual cortex

Van der Loos, 1970). Neurons in the barrels and septa are known to be associated with distinct thalamocortical and intracortical circuits and display different receptive field properties (Koralek et al., 1988; Lu and Lin, 1993; Kim and Ebner, 1999; Brecht and Sakmann, 2002; Brecht et al., 2003). Short-tailed opossums, on the other hand, lack any histologically detectable barrels or septa in S1 (Huffman et al., 1999; Wong and Kaas, 2009). This is not an anomaly; many animals that possess whiskers do not have detectable barrels in the cortex (Woolsey et al., 1975), although barrel-like structures may be present at subcortical levels, for example, in cats and other carnivores (Nomura et al., 1986) and in water shrews (Catania et al., 2013).

The functional organization of barrel cortex in rats and mice has been described in great detail; there is a precise spatiotopic map of the whisker array in layer IV of S1, such that neurons in each barrel respond primarily to a single best whisker (BW; Welker, 1971, 1976; Simons, 1978). Neurons also frequently display a much lower magnitude response to other, surrounding whiskers (Armstrong-James and Fox, 1987; Welker et al., 1996). Furthermore, there is a clear temporal segregation of the responses to the BW and surrounding whiskers, with surround responses having longer latencies than the responses to the BW (Armstrong-James and Fox, 1987; Welker et al., 1996). It is unknown whether these receptive field and response properties are features of somatosensory cortex that are also present in other mammals, including those species that naturally lack barrel-like parcellation of S1 whisker cortex.

This study quantitatively examines the spatial and temporal response characteristics of single neurons in the S1 whisker representation of short-tailed opossums. We seek to elucidate basic features of sensory processing during whisker-mediated touch that are similar or different in marsupial and placental species, with the ultimate goal of identifying common principles of organization of neural circuits in S1 that can be generalized across all mammalian species.

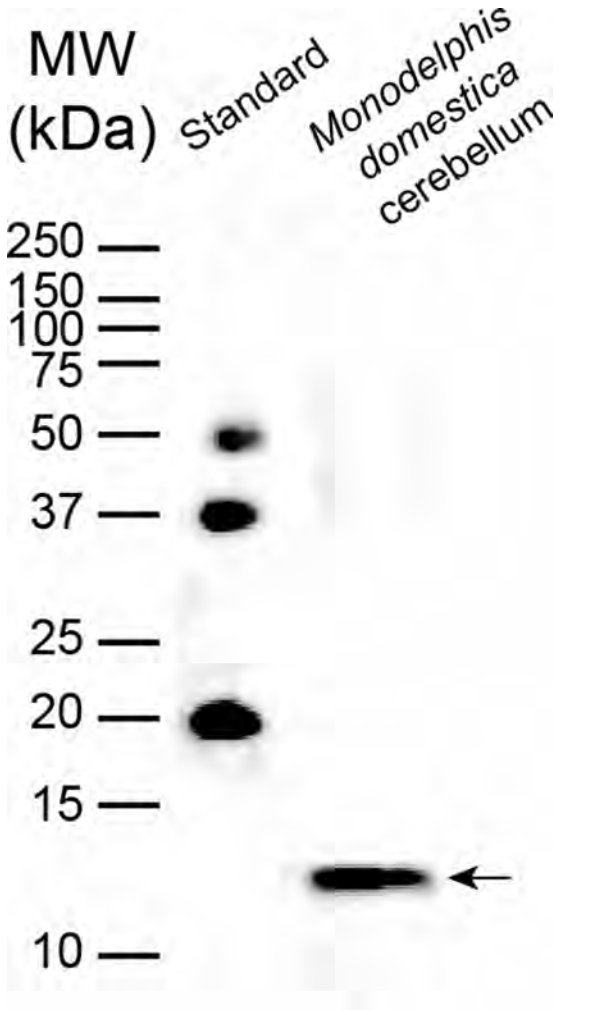

Figure 1. Western blot characterization of the antiparvalbumin antibody. A single protein band (arrow) is detected at 12–13 kDa in short-tailed opossum cerebellar lysate; this is within the expected molecular weight range of the parvalbumin protein.

MATERIALS AND METHODS

Subjects

Eleven adult short-tailed opossums were used in the current study. Nine animals (five males and four females, 85–126 g) were used in electrophysiological recording experiments. One animal was used for additional histology, and another animal was used for Western blot analysis (Fig. 1). The animals were housed in standard laboratory cages in which food and water were available *ad libitum*, and were maintained on a 14/10-hour light/dark cycle. All experiments were performed according to the criteria outlined in the National Institutes of Health *Guide for the Care and Use of Laboratory Animals*, and all protocols were approved by the Institutional Animal Care and Use Committee (IACUC) of the University of California, Davis.

Electrophysiological recordings

At the start of the experiment, animals were anesthetized with urethane (1.25 g/kg, 30% in propylene glycol, IP). Supplemental doses of urethane (0.125–0.3125 g/kg, 30% in propylene glycol, IP) were provided when required. Respiration and body temperature were monitored throughout the surgery. Animals were given dexamethasone (0.4–2.0 mg/kg, IM) at the beginning of the surgery. Lidocaine (2% solution) was subcutaneously

injected at the midline of the scalp and around the ears, and the animal was placed in a stereotaxic frame. An incision was made at the midline of the scalp, the temporal muscle was retracted, and a craniotomy was performed such that the parietal cortex was exposed. The head of the animal was stabilized with a skull screw cemented to a head post. The dura was retracted, and the brain was covered with silicone fluid to keep it moist and insulated during the recording session. A digital image was taken of the exposed neocortex so that electrode penetration sites could be directly related to vascular patterns.

Extracellular recordings were made from layer IV (400–500-μm depth below the pial surface) with insulated tungsten microelectrodes (1–5 MΩ at 1 kHz; FHC, Bowdoin, ME; A-M Systems, Sequim, WA). Electrodes were lowered using either a hydraulic microdrive (David Kopf Instruments, Tujunga, CA) or a manually controlled micromanipulator (World Precision Instruments, Sarasota, FL). The location of each recording site was marked on a digital image of the cortical surface relative to the vascular pattern.

First, receptive fields were coarsely mapped with a handheld probe. After this, when receptive fields were found to be located on the mystacial or genal whisker pad (Fig. 2A–D), computer-controlled whisker deflections (see below) were used to measure receptive field tuning quantitatively (Fig. 3A–D). Single- and multiunit activity was recorded in response to whisker deflections, and all recorded data were amplified (×10,000 gain; model 1800 microelectrode AC amplifier; A-M Systems, Carlsborg, WA), streamed as continuous voltage traces sampled at 28 kHz (Power1401; Cambridge Electronic Design Limited, Cambridge, United Kingdom), and saved for analysis. Neural activity was monitored through a loudspeaker and viewed on a computer screen during the experiment. Raw traces were bandpass filtered (300–3,000 Hz), and spike sorting was carried out offline to isolate single units.

At the end of the recording session, fluorescent probes were inserted at specific locations relative to blood vessel landmarks so that electrophysiological recording sites could be related to cortical vasculature and myeloarchitecture. In one case, electrolytic microlesions (10 μA for 10 seconds) were also placed at known depths to aid in the reconstruction of the laminar and areal positions of recording sites.

Whisker stimulation

At each recording site, neural responses to somatosensory stimulation (consisting of light taps, displacement of whiskers, brushing of skin, hard taps, and manipulation of muscles and joints) were tested with a handheld probe. When responses were driven by the deflection of either the mystacial whiskers or the genal whiskers, receptive fields and response properties were quantified as described below.

Whiskers were deflected with computer-controlled piezoelectric actuators (Fig. 3A). The piezoelectric device was calibrated with a photodetector circuit (Fig. 3B). Whiskers were trimmed to a length of 15 mm. Each individual whisker was inserted into a short, lightweight plastic capillary tube glued to a piezoelectric bimorph element (Q220-AY-203YB; Piezo Systems, Woburn, MA) fixed on a moveable, jointed arm. The piezoelectric device was positioned such that the whiskers were maintained at their initial resting position and angle. During stimulus presentation, the piezoelectric device was carefully observed under a surgical microscope to ensure that it did not touch the skin or whiskers adjacent to the stimulated whisker.

Stimuli consisted of 2° ramp–hold–return deflections (10-msec ramp, 100-msec hold, 10-msec return; applied 5 mm from the base of the whisker, causing a 1.4 mm excursion of the whisker from its resting position) with an interstimulus interval of 1 or 2 seconds. For a subset of recording sites, a range of deflection amplitudes (0.1 – 2.0°) was tested to obtain a stimulus strength–response function. Additionally, stimuli with shorter rise/fall times (4-msec ramp, 100-msec hold, 4-msec return) were tested for a subset of recorded neurons. Twelve, twenty-five, or fifty trials per stimulus per whisker were collected at each recording site. To construct spatial receptive fields, 15–19 neighboring whiskers on the mystacial pad were deflected at every recording site. Except in one animal (for which short whiskers were glued to the capillary tube while being stimulated), receptive fields were not quantified if they were centered on the rostralmost two or three mystacial whiskers in rows C and D (Fig. 2D) because these whiskers were too short to be held firmly in the piezoelectric device. When a receptive field was located on the genal whiskers, all seven genal whiskers were tested. For data included in this study, all whisker deflections were performed along the rostrocaudal axis.

Histology

After electrophysiological recording experiments, animals were euthanized with an overdose of sodium pentobarbital (Beuthanasia; 250 mg/kg, IP) and transcardially perfused with 0.9% saline, followed by 2–4% paraformaldehyde in phosphate buffer and then 2–4% paraformaldehyde in 10% phosphate-buffered sucrose. After perfusion, the brain was extracted, and the cortical hemispheres were separated from subcortical structures. The dissected hemispheres were

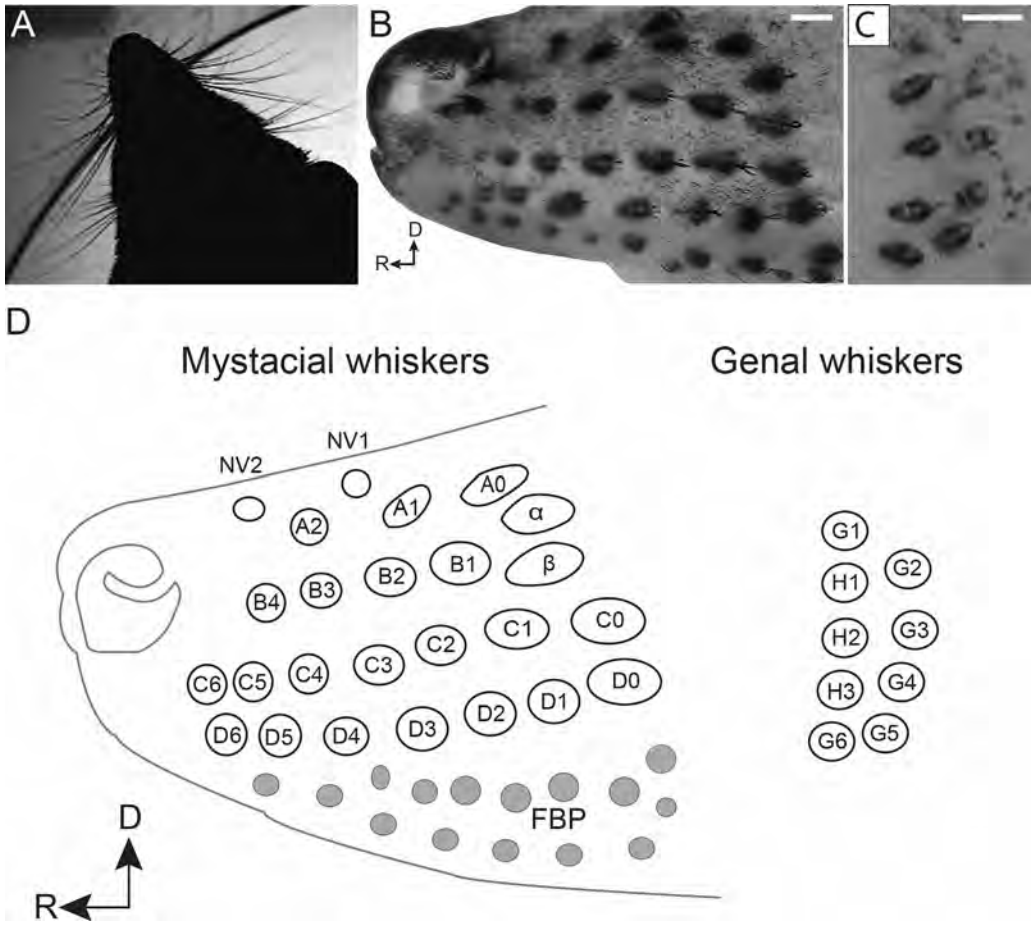

Figure 2. Arrangement of the large facial whiskers in *M. domestica*. **A:** Dorsal view of a whisking short-tailed opossum in silhouette shows the position of the mystacial whiskers on the snout and the genal whiskers on the cheeks. Supraorbital, submental, and interramal whiskers are also present in short-tailed opossums but were not studied in the current work. **B:** Mystacial whisker follicles revealed in an ethanol/xylene-cleared preparation of the mystacial pad. D, dorsal; R, rostral. **C:** Whisker follicles revealed in an ethanol/xylene-cleared preparation of the genal pad. **D:** Schematic illustration of the whisker pad in *M. domestica* (adapted from Grant et al., 2013). Twenty-three mystacial whiskers are named after their row (A–D) and arc (0–6) position and are highly stereotyped in their number and location, with 3–7 whiskers in each row. Two straddler whiskers are present, α and β. Nasal whiskers (NV1, NV2) are found dorsal to the mystacial pad. The FBP is located ventral to the mystacial pad. Unlike the mystacial whiskers, the number of genal whiskers is variable, with five to ten whiskers located caudal to the mystacial pad, arranged in vertical groups with one or two arcs (G,H). They are named after the arc in which they are located and their numeric position within the arc (1 being the most dorsal). D, dorsal; R, rostral. Scale bars = 2 mm.

flattened between glass slides, postfixed briefly in 4% paraformaldehyde in 10% phosphate-buffered sucrose, and then left to soak overnight in 30% sucrose. The flattened cortical hemispheres were sectioned at 30 μm on a freezing microtome. In one case used exclusively for histology (Fig. 4A–C), alternating tangential sections were processed for cytochrome oxidase (Wong-Riley and Welt, 1980; Wong, 1989) and myelin (Gallyas, 1979; Dooley et al., 2013; Fig. 4A–C); in the other cases, myelin staining was used on tangential sections of the neocortex (Fig. 5A–C). In one case, the entire brain was cut coronally into 40-μm sections. Alternating coronal sections were processed for parvalbumin expression (mouse monoclonal antiparvalbumin; 1:2,000; catalog No. P3088; RRID:AB_477329; Sigma-Aldrich, St. Louis, MO; Wong and Kaas, 2009) or Nissl substance and used for reconstructing the position of recording sites (Fig. 6A–C). When required, entire digital images were adjusted for contrast and brightness in Photoshop CS5 (Adobe Systems, San Jose, CA).

Antibody characterization

We used parvalbumin immunohistochemistry to aid in the identification of areal and laminar boundaries of S1, in addition to Nissl and myelin staining. Table 1 provides information about the antibody used in the

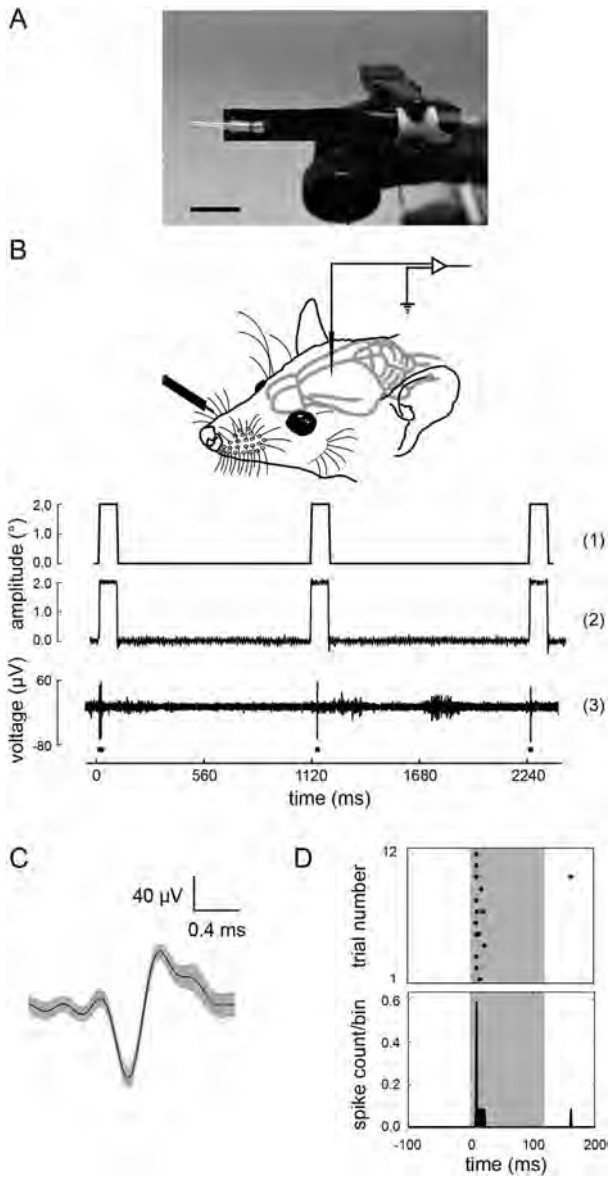

Figure 3. Experimental design. **A:** Photograph showing the piezoelectric whisker stimulator. **B:** Schematic showing the electrophysiological recording setup. Trace 1 shows the computer-generated ramp–hold–return signal (10-msec ramp, 100-msec hold, 10-msec return) on three consecutive trials. Trace 2 shows the movement of a whisker with the piezoelectric device, calibrated using a photodetector circuit. Trace 3 shows extracellular activity recorded from somatosensory cortex in response to the deflection of an individual whisker on the contralateral face with the computer-controlled piezoelectric device. Spikes evoked in response to whisker deflection in a single neuron are indicated by dots beneath the voltage trace. **C:** Average spike waveform for the neuron shown in B indicates good single-unit isolation. Shaded region represents the SD of the mean. **D:** Raster plot and PSTH obtained for the neuron (same as shown in B,C) across 12 trials. Shaded region indicates the duration of the stimulus. Scale bar = 10 mm.

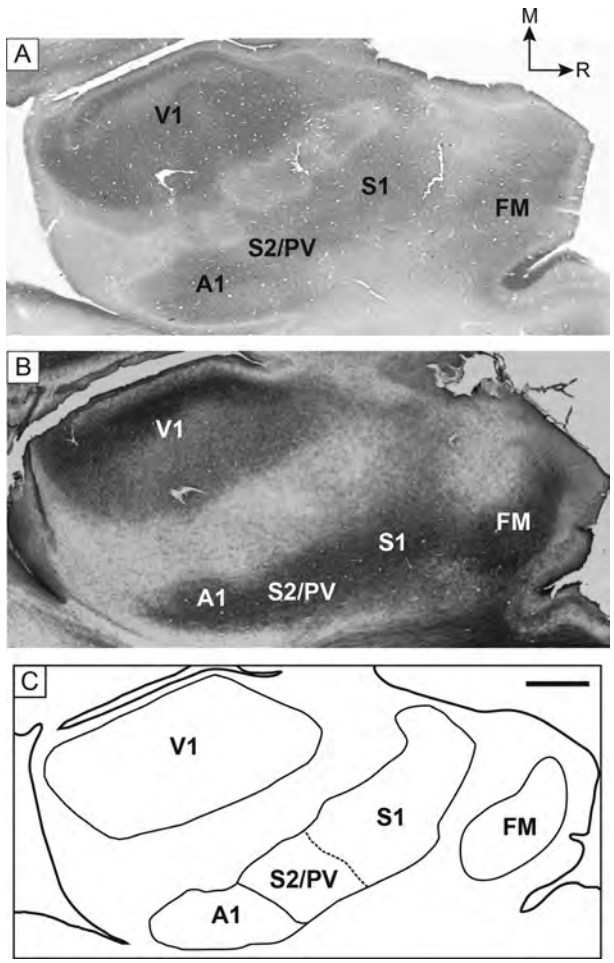

Figure 4. Architectural boundaries of S1 and surrounding cortex. **A:** Cytochrome oxidase stain of a tangential section of the neocortex. Regions of the cortex that stained dark with cytochrome oxidase were in alignment with densely myelinated regions of the cortex (**B**), including primary sensory areas. Cytochrome oxidase staining within S1 is uniformly dark; no whisker-related patterns are identifiable. **C:** Reconstruction of architectural boundaries drawn from an entire series of sections. M, medial; R, rostral. Scale bar = 1 mm.

current study. The pattern of parvalbumin expression within short-tailed opossum cortex was comparable to the patterns previously reported for the same antibody in the same species (Wong and Kaas, 2009). The specificity of this antiparvalbumin antibody in short-tailed opossums has previously been reported (Olkowicz et al., 2008). We verified these findings by performing Western blot analysis with standard procedures. One animal was deeply anesthetized with isoflurane and decapitated. The brain was rapidly extracted, and cerebellar hemispheres were dissected out, placed in microcentrifuge tubes, frozen on dry ice, and stored at –80°C until processing. Proteins in the cerebellar tissue lysate were separated with gel electrophoresis. Subsequent to

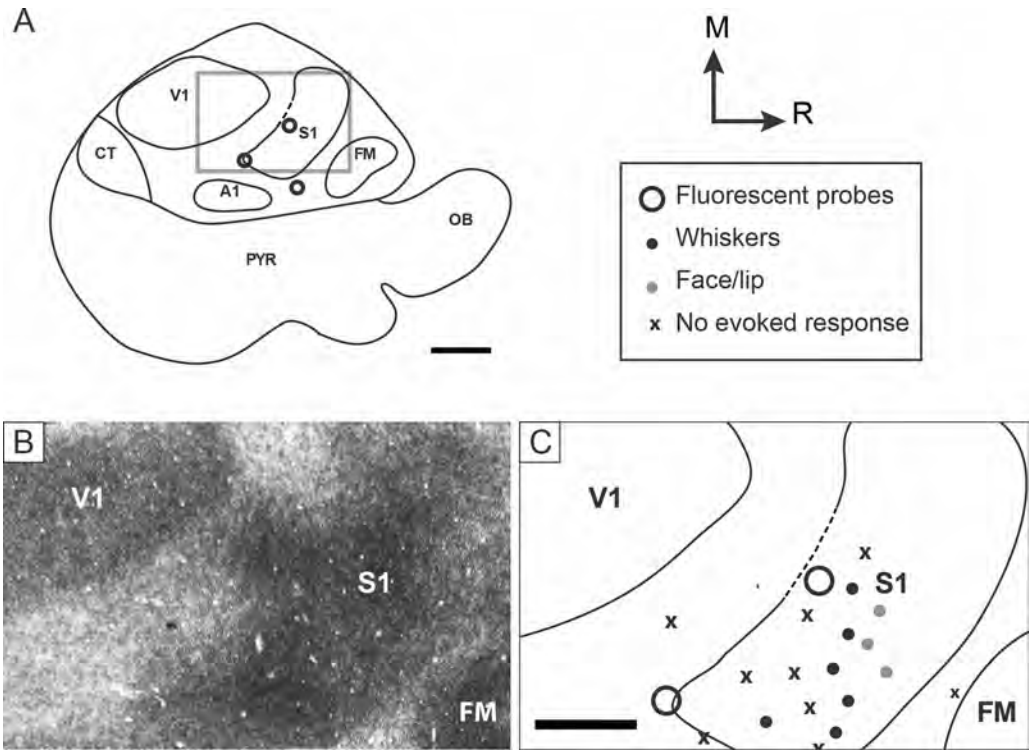

Figure 5. Relation of electrophysiological recording sites to architectonically determined borders of S1. **A:** Reconstruction of myeloarchitectural boundaries on a tangential section of the cortex. These boundaries were drawn from an entire series of sections. The location of fiducial probes is indicated by circles, and the region corresponding to images in B,C is outlined in gray. M, medial; R, rostral. **B:** Myelin stain of the outlined region in the tangential section shown in A. **C:** Location of electrode penetrations relative to architectural boundaries of S1 for the section shown in B. S1 is readily distinguished from adjacent cortex by its dark myelination. Scale bars = 2 mm in A; 1 mm in C (applies to B,C).

electrophoretic separation, the proteins were transferred from the gel to a membrane that was removed and incubated overnight at 2–4°C in the primary antibody, mouse monoclonal antiparvalbumin (P3088; Sigma), diluted to a concentration of 1:2,000 in Tris-buffered saline with Tween 20 and 5% nonfat dry milk, and incubated for 1 hour with HRP-conjugated horse anti-mouse IgG antibody (1:2,000; PI-2000; Vector Laboratories, Burlingame, CA). The resulting protein bands were visualized via ECL detection with Clarity Western ECL substrate (Bio-Rad, Hercules, CA). Just as in a previously published study (Olkowicz et al., 2008), a single band of labeled protein was clearly visible at approximately 12 kDa, the molecular weight of parvalbumin (Fig. 1).

Whisker pad processing

In two cases, the whisker pad was processed to visualize the organization of whisker follicles in the mystacial pad and genal areas (Grant et al., 2013; Fig. 2B,C). These portions of the facial skin were removed, shaved, scraped to remove fatty tissues, flattened, and dehydrated in a series of ethanol washes with decreasing concentrations of water (50%, 70%, 95%, and 100% ethanol). These were then submerged in xylene until the samples turned clear. The xylene-cleared samples were backlit with a light box and photographed with a Nikon (Tokyo, Japan) D5100 camera. When required, contrast and brightness of entire digital images were adjusted in Photoshop CS5 (Adobe Systems).

Statistical analysis

Single units were isolated using template-matching procedures, principal component analysis, and inspection of interspike interval (ISI) histograms (<0.1% of spikes with ISIs of <1-msec) in Spike2 (Cambridge Electronic Design Limited, Cambridge, United Kingdom). Measurements of spike duration were made from the average spike waveform for each unit. In the current study, we did not distinguish between excitatory and inhibitory neurons based on physiological properties; data from neurons with short and long spike durations were combined for population analyses because they could not readily be distinguished as distinct populations of neurons from spike duration alone. Spike times of well-isolated single units were exported to MATLAB (MathWorks, Natick, MA) for analysis with custom

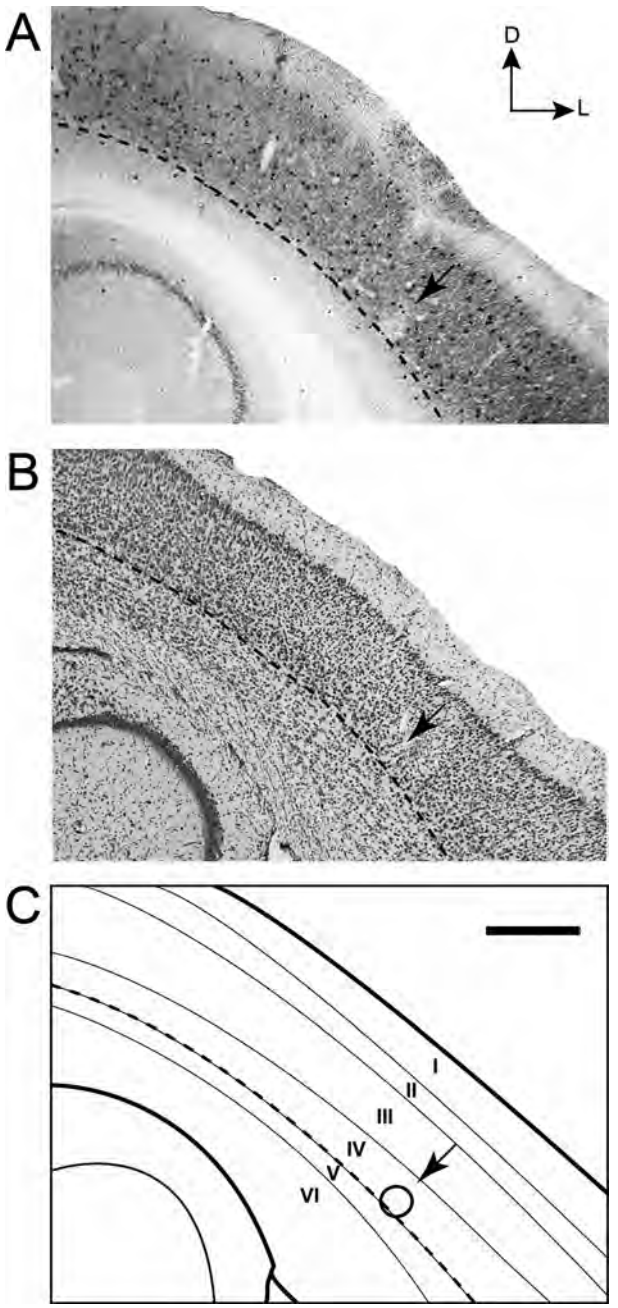

Figure 6. Relation of electrophysiological recording sites to laminar borders of S1. Coronal sections of the brain stained for parvalbumin (**A**) and Nissl (**B**) with an electrolytic lesion made at a recording site (arrows), visible in layer IV of the cortex (B). D, dorsal; L, lateral. **C:** Reconstruction of laminar boundaries from these coronal sections of the cortex with the location of the electrolytic lesion indicated by the circle. The dashed lines in A–C mark the ventral boundary of layer IV. Scale bar = 250 μm.

scripts. Spike trains were aligned to the time of onset of the computer-generated ramp signal, and peristimulus time histograms (PSTHs) were constructed with a 1-msec bin width (Figs. 7A–C, 8A–C). Neural responses were quantified over a 75-msec time window following stimulus onset or offset (Figs. 9A–D, 10A–C). Receptive field analysis was performed only for onset responses. Response magnitude was calculated based on the spike count after deflection onset (0–75 msec). Spontaneous firing rates were measured for an equivalent time during the prestimulus recording period. A neuron was considered to exhibit a significant evoked response if the response magnitude exceeded the prestimulus spike count by more than 2 SDs. Neural responses detected with this threshold were in agreement with visual inspection of PSTHs. Only neurons that displayed a significant onset response to at least one whisker were included in the remaining analyses. The BW for a neuron was defined as the whisker that evoked the highest response magnitude. Response magnitudes were corrected for spontaneous firing rates. The whiskers at the eight positions immediately adjacent to the BW (rostral, caudal, dorsal, ventral, rostrodorsal, caudodorsal, rostroventral, and caudoventral) are referred to as first-order adjacent whiskers, and the whiskers immediately beyond those are referred to as second-order adjacent whiskers.

Mean receptive fields were constructed after aligning the receptive fields of the individual neurons such that the BW was at the center of the receptive field in each case. The response magnitude to the stimulation of each first-order adjacent whisker in the receptive field was normalized by dividing it by the BW response magnitude. Contour plots (generated after smoothing the response magnitude matrix by linear interpolation) were used to visualize individual as well as mean receptive fields (Figs. 11A–E, 12A–D). The tuning width index for each neuron was calculated as the mean response to stimulation of the first-order adjacent whiskers divided by the BW response (Fig. 12E). Higher tuning width indices indicate broader receptive fields. When a whisker was absent at any of the first-order whisker positions, those values were considered to be missing, and means were calculated without including those values. This was required because there are only five positions (from among 25) in the short-tailed opossum mystacial whisker pad (B1, B2, C1, C2, and C3) at which whiskers are present at all eight adjacent positions, and we did not restrict data collection to neurons that had their BWs at those five positions. The mean receptive field was also separately computed for the subset of neurons (7/70 neurons) for which surrounding whiskers were tested at all eight positions immediately adjacent to the BW. In addition to the overall tuning width index, a row tuning width index calculated as the mean response of the adjacent whiskers in the same row as the BW (in-row surround whiskers), divided by the BW response and an arc tuning width index calculated as

TABLE 1.
Antibody Characterization

Antigen	Immunogen	Source, host species, catalog No., RRID	Dilution factor
Parvalbumin	Purified frog muscle parvalbumin	Sigma-Aldrich, mouse monoclonal antiparvalbumin, P3088, AB_477329	1:2,000

the mean response of the two adjacent whiskers in the same arc as the BW (in-arc surround whiskers), divided by the BW response were also calculated. These were used to calculate the shape index for each neuron, defined as the difference between the row tuning width index and the arc tuning width index divided by their sum (Figs. 12F, 13A–D). For cases in which the sum of the row and arc tuning width indices was zero, the shape index was assigned to be zero. Shape index values range from −1.0 to +1.0, with positive values indicating broader tuning along the row compared with the arc, and negative values indicating broader tuning along the arc compared with the row.

Population average PSTHs (Fig. 14A) were smoothed with a 3-msec moving average for the purpose of visualization. Latency measures were computed from unsmoothed PSTHs. All latency values are reported relative to the onset of movement of the piezoelectric device. Two measures of response latency (Fig. 14A–G) were used when significant evoked responses were observed: 1) onset latency (time of occurrence of the first 1-msec bin of the PSTH that contained a firing rate greater than 2 SDs above spontaneous firing) and 2) peak latency (the time of the 1-msec bin of the PSTH that contained the maximum number of spikes). Statistical analyses were performed in Matlab 8.1.0 (Mathworks) and R 3.2.0 (R Development Core Team 2015). Summary data are reported as mean ± standard error, or median ± standard error. The Kolmogorov-Smirnov test was used to compare firing rate distributions. For each parameter, normality of the distribution was assessed with the Shapiro-Wilks test. Two-sample *t*-tests were used to compare population means, and paired-sample *t*-tests were used to make comparisons for paired data. Whenever assumptions of normality were not met, statistical analyses were repeated with nonparametric tests (Wilcoxon rank-sum test to compare population medians and Wilcoxon signed-rank test for matched pair comparisons). Bonferroni's correction was used when multiple comparisons were made. A nonparametric multivariate analysis of variance (MANOVA) was used to check for influences of sex and individual differences on response magnitude, onset latency, peak latency, tuning width index, and shape index. $P < 0.05$ was considered to be statistically significant.

RESULTS

This study quantitatively characterizes the receptive fields and response properties of single neurons in S1 of short-tailed opossums. Across nine animals, we made extracellular recordings of neural activity from 107 single units in response to the computer-controlled deflection of individual whiskers. Fifteen to nineteen neighboring mystacial whiskers or all seven genal whiskers were tested for each unit. 70 from among 107 units exhibited a significant evoked response to the deflection of at least one mystacial or genal whisker, and these were used in the analyses of the spatial and temporal response characteristics of neurons in S1. A summary of the sampling of responsive neurons is provided in Table 2. For the parameters examined (see Materials and Methods), no statistically significant differences were found between sexes or among animals, so all data were combined for analysis.

Whisker pad morphology

In *M. domestica*, the large facial whiskers are arranged in a grid-like pattern consisting of horizontal rows and vertical arcs, with an overall organization similar to that of rats and mice. Direct comparisons between the whisker pad morphology of short-tailed opossums and that of other mammals, including rats and mice, have been made in previous studies (Brecht et al., 1997; Grant et al., 2013). In addition to the mystacial whiskers on the snout (23 per side), short-tailed opossums also possess a set of genal whiskers (five to 10 per side) in the cheek region that are absent in rats and mice but are present in all examined species of marsupials (Lyne, 1959; Fig. 2A–D). Facial whiskers are also present at supraorbital, interramal, and submental positions in short-tailed opossums but are generally less prominent and were not investigated in the current study. We visualized the arrangement of the mystacial and genal whiskers in short-tailed opossums with an ethanol/xylene-cleared preparation of the whisker pads (Fig. 2B,C), as previously described by Grant and colleagues (2013), to get a clear depiction of the peripheral morphology of the whisker system. The nomenclature used in this study for referring to specific whiskers is adapted from Grant and colleagues (2013). The mystacial whiskers in short-tailed opossums were

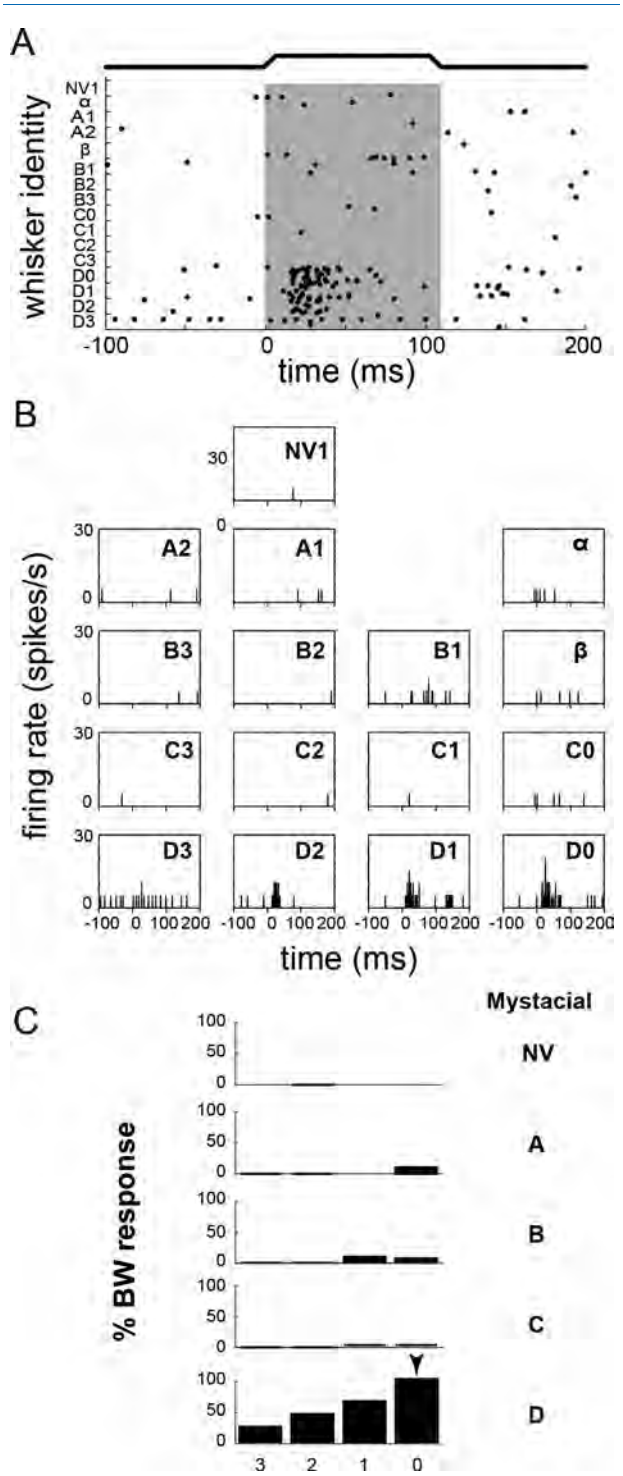

Figure 7. Responses of a single neuron in S1 with a receptive field on the mystacial whiskers. **A:** Spike raster plot for a neuron in S1 in response to the stimulation of 16 individual mystacial whiskers. Shaded region indicates duration of the stimulus. **B:** PSTHs of the same neuron in response to the deflection of the different mystacial whiskers. **C:** Magnitude of the neuronal response (integrated spike count, 0–75 msec) to each whisker, visualized as a percentage of the BW response. Arrow indicates BW (D0).

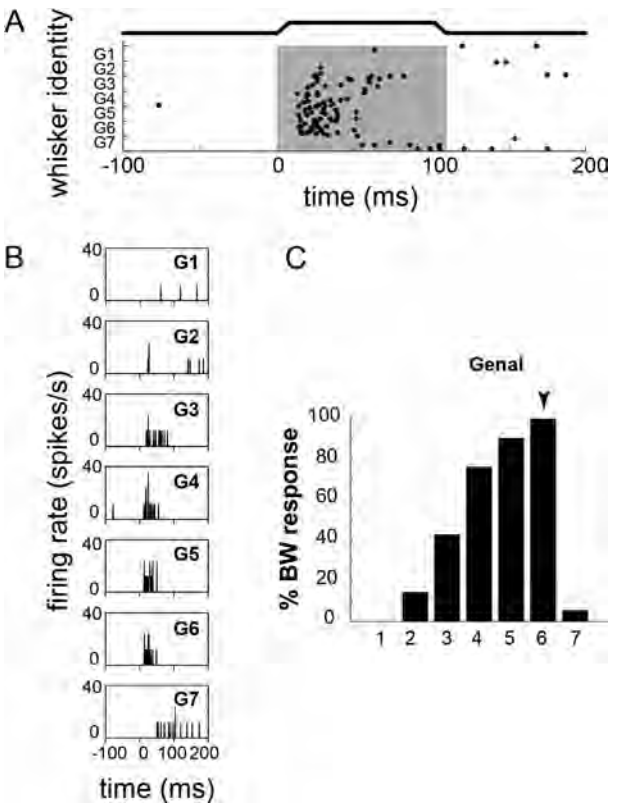

Figure 8. Responses of a single neuron in S1 with a receptive field on the genal whiskers. **A:** Spike raster plot for a neuron in S1 in response to the stimulation of seven individual genal whiskers. Shaded region indicates duration of the stimulus. **B:** PSTHs of the same neuron in response to the deflection of the different genal whiskers. **C:** Magnitude of the neuronal response (integrated spike count, 0–75 msec) to each whisker, visualized as a percentage of the BW response. Arrow indicates BW (G6).

arranged in a well-defined grid of four rows (A–D, dorsal to ventral) and six arcs (0–6, caudal to rostral) along with two straddler whiskers (α and β) located on both sides of row B (Fig. 2B,D). The mystacial whiskers were highly stereotypical in their number and placement on the snout. The dorsal two rows of mystacial whiskers had fewer whiskers (three in row A, four in row B) than the ventral two rows (seven each in row C and row D). The α whisker was situated between rows A and B, and the β whisker was situated between rows C and D. In general, mystacial whiskers increase in size (diameter and length) from rostral to caudal positions and from dorsal to ventral positions. Two nasal whiskers (NV1 and NV2) were located dorsal to the mystacial whiskers, and several small sinus hairs constituting the furry buccal pad (FBP) were located ventral to the mystacial whiskers. The genal whiskers were arranged in one or two arcs (G and H; 0–5 or higher indices [see

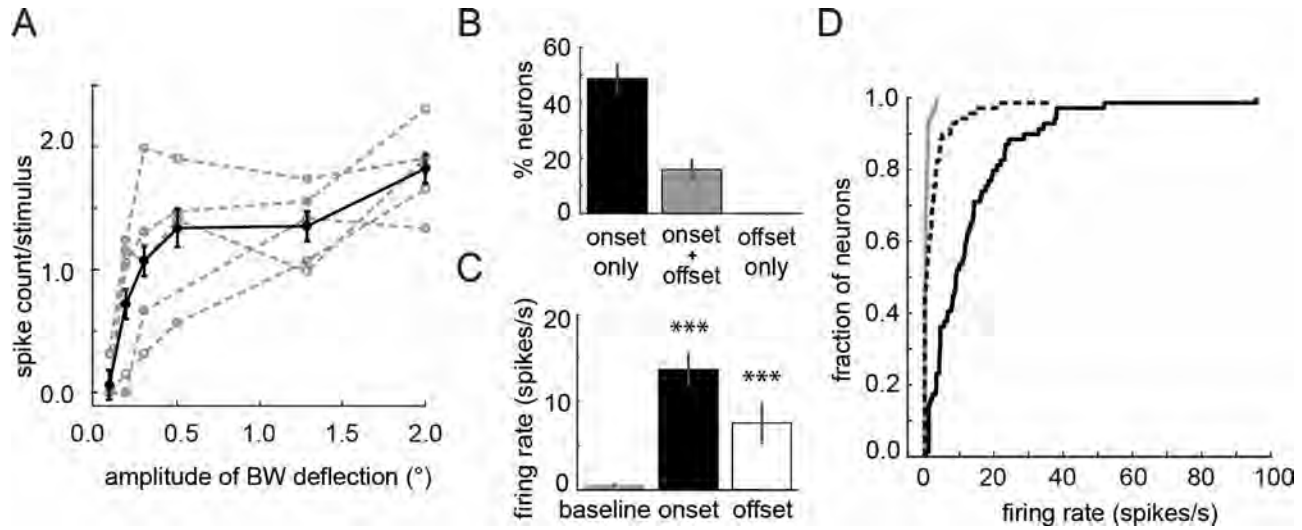

Figure 9. Summary of spontaneous and evoked firing rates. **A:** Mean stimulus strength–response function for five different layer IV neurons (solid line), plotted for incremental deflections (0.1–2.0°) applied to the BW. Response functions for the individual neurons are also shown (dashed lines). Stimuli were applied at a distance of 5 mm from the face. Response magnitudes were measured as spike counts 0–75 msec following stimulus onset, averaged across trials (12, 25, or 50). **B:** Percentages of recorded units (n = 107) that display a significant response to stimulus onset only (solid bar, 49%), both stimulus onset and offset (shaded bar, 17%), and stimulus offset (0%). Error bars show standard error of the proportion. **C:** Comparison of the mean prestimulus spontaneous firing rate (shaded bar) and evoked firing rates during the onset period (solid bar) and the offset period (open bar). Error bars show SEM. ***$P < 0.001$, significant differences of onset and offset firing rates relative to spontaneous activity (two-sample *t*-test, Wilcoxon rank-sum test). **D:** Cumulative distributions of spontaneous (gray line) and onset (black line) and offset (dashed line) period firing rates for the neurons included in receptive field analyses (onset responsive neurons, n = 70). Spontaneous firing rates were low. Onset and offset spike counts were measured in a 75-msec time window following stimulus onset and offset, respectively, and were considered to be significant if they exceeded 2 SDs above the spontaneous spike count in a 75-msec prestimulus window. Analysis of spatial and temporal response characteristics was performed only for onset responses.

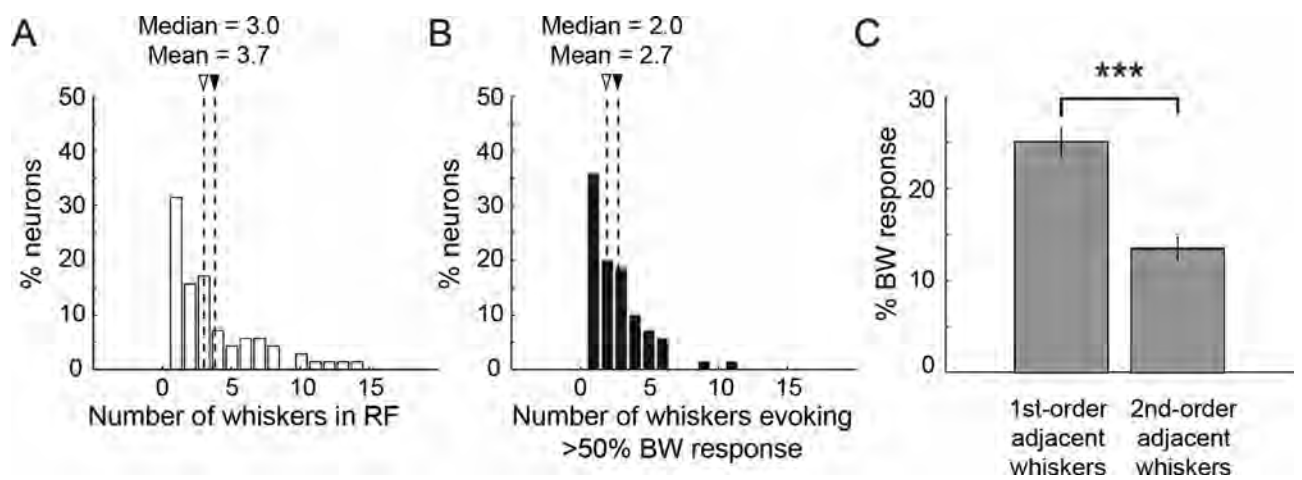

Figure 10. Summary of receptive field sizes. **A:** Distribution of receptive field sizes of single neurons measured as the number of whiskers that evoke a significant response above spontaneous activity. Among responsive S1 neurons (n = 70), 31% responded only to a single whisker; the remaining 69% of neurons displayed multiwhisker receptive fields. **B:** Distribution of the number of whiskers in each receptive field evoking a response greater than 50% of the BW response. For 64% of neurons, more than one whisker elicited a response greater than half the magnitude of the BW response. Open arrowhead indicates median value; solid arrowhead indicates mean value. **C:** Comparison of the mean response magnitude (relative to the BW) of first-order adjacent whiskers and second-order adjacent whiskers. Error bars show SEM. There was a significant decrease in the magnitude of the neural response between first-order and second-order adjacent whiskers. ***$P < 0.001$, two-sample *t*-test, Wilcoxon rank-sum test.

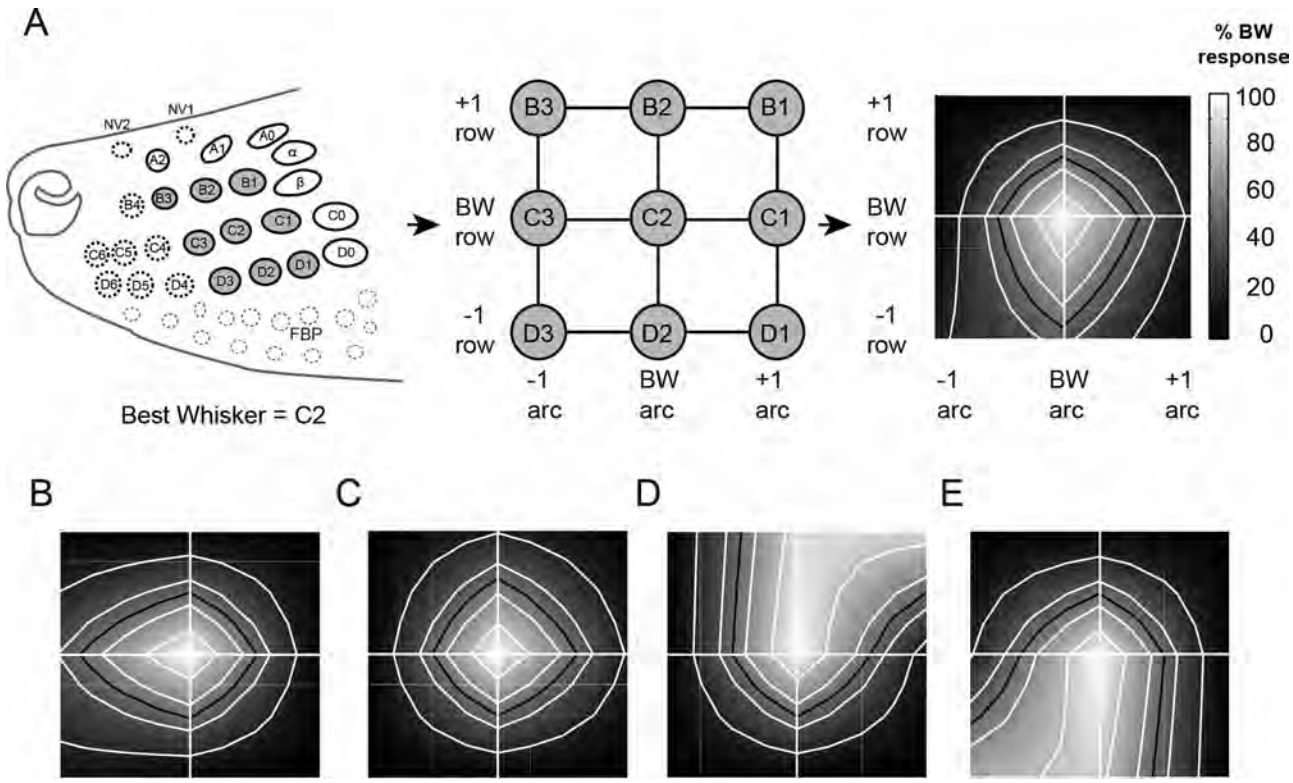

Figure 11. Receptive field configuration of single neurons in S1. **A:** Visualization of the receptive field of an example neuron, with C2 as the BW. At left is an illustration of the mystacial pad. All tested whiskers are encircled with solid lines, whereas untested whiskers are encircled with dashed lines. For this example, the BW and eight immediately surrounding whiskers are indicated by gray fill. In the center is a schematic representation of the BW and eight surrounding whiskers as a 3 × 3 grid. At right is the contour plot obtained with the response magnitudes to the stimulation of each of the whiskers in the 3 × 3 grid. The spatial configuration of the receptive field was examined by considering the response magnitude of the BW (center of the receptive field) and the eight immediately adjacent surrounding whiskers. White contour lines show 20%, 40%, 60%, and 80% response levels (relative to the BW). Black contour line shows the 50% response level (half-height of the two-dimensional tuning curve). **B–E:** Examples of contour plots of the receptive fields for four additional neurons. Although we observed different shapes of receptive fields (e.g., D,E), the most common receptive field shape was oval or round.

below], dorsal to ventral) on the cheek (Fig. 2C,D). Although they were always present as a vertically arranged group in the cheek region, the genal whiskers showed interindividual variability in number and position, unlike the stereotypically arranged mystacial whiskers. For consistency, the genal whisker at the most dorsal position was considered to be the G1 whisker, and remaining genal whiskers were identified from their position relative to this whisker.

We examined the responses of neurons in S1 to stimuli that were applied to the mystacial as well as genal whiskers. Quantitative data were not collected when receptive fields were centered on the rostralmost two or three mystacial whiskers in the C-row and D-row because those whiskers were too short to be secured in the piezoelectric actuator device. Apart from that, we did not restrict data collection to neurons that had their receptive fields on any specific portion of the whisker array.

Qualitative assessment of receptive fields

For every recording site, a handheld probe was first used to qualitatively assess receptive fields while monitoring unit activity with an oscilloscope and audio monitor. Neural responses were tested for the deflection of all mystacial and genal whiskers on both ipsilateral and contralateral sides as well as the skin and fur on the snout in the region adjacent to and between the whiskers. For neurons that responded to whisker deflection, responses were evoked only by whiskers on the contralateral side; stimulation of ipsilateral whiskers and adjacent skin and fur failed to evoke detectable responses under our recording conditions. Mystacial and genal whiskers did not, in any case, evoke responses in the same neurons. At some sites, evoked responses could be detected only in response to the deflection of a single whisker, whereas, at other sites, multiple whiskers were found to elicit a response. When a receptive field was found to span more than one whisker,

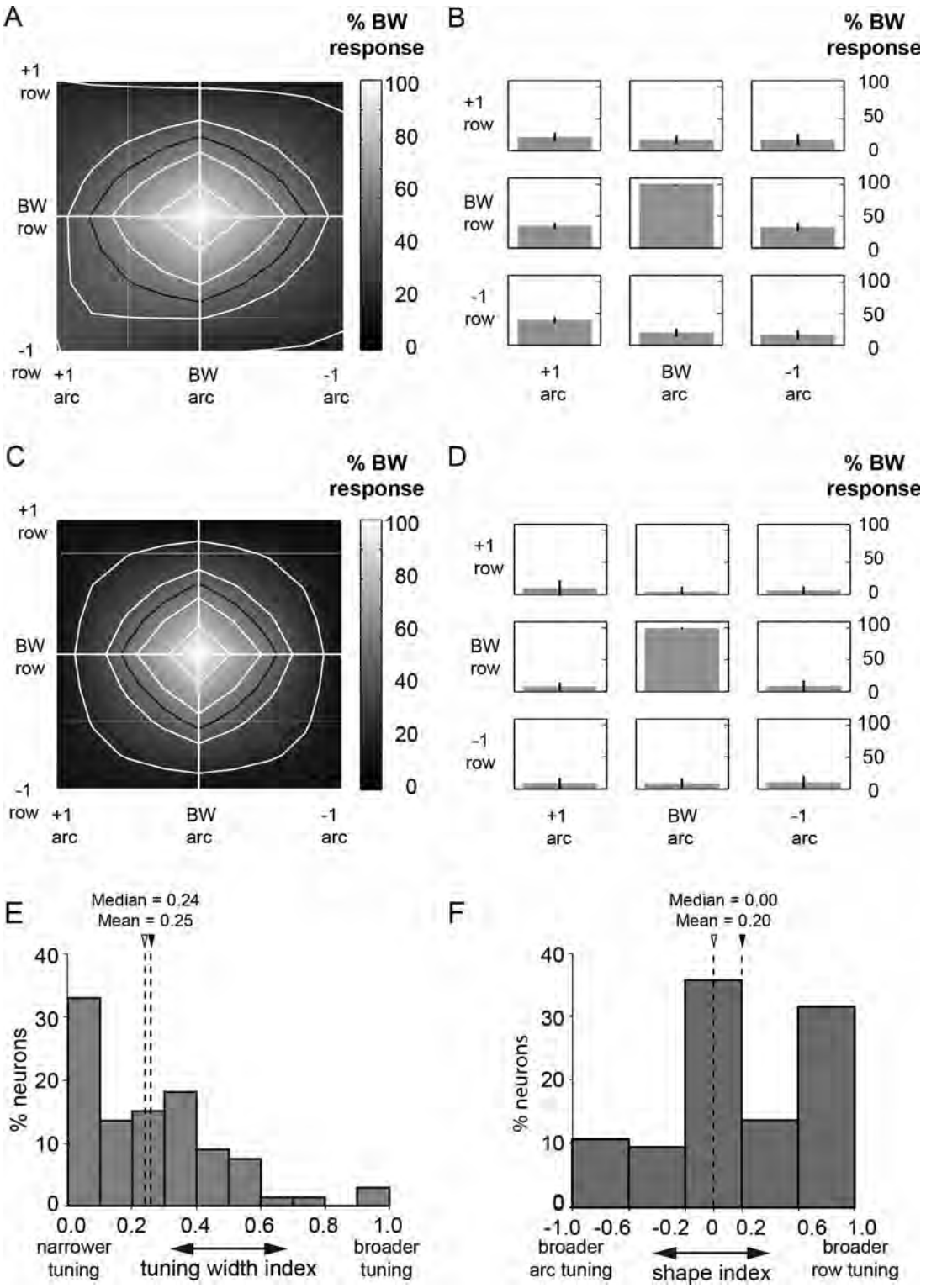

Figure 12. Mean receptive field configuration. **A:** Average single neuron receptive field (n = 70). The contour plot is centered on the BW. **B:** Data from A visualized with a bar chart; error bars show SEM. **C:** Average single neuron receptive field contour plot including only neurons for which whiskers were present at all eight positions surrounding the BW (n = 7). **D:** Data from C visualized with a bar chart; error bars show SEM. **E:** Tuning width index distribution for the whole data set. Higher tuning width index values indicate broader receptive fields. **F:** Shape index distribution for the whole data set. Positive values indicate broader tuning along the row of the BW, and negative values indicate broader tuning along the arc of the BW. Open arrowhead indicates median value, solid arrowhead indicates mean value.

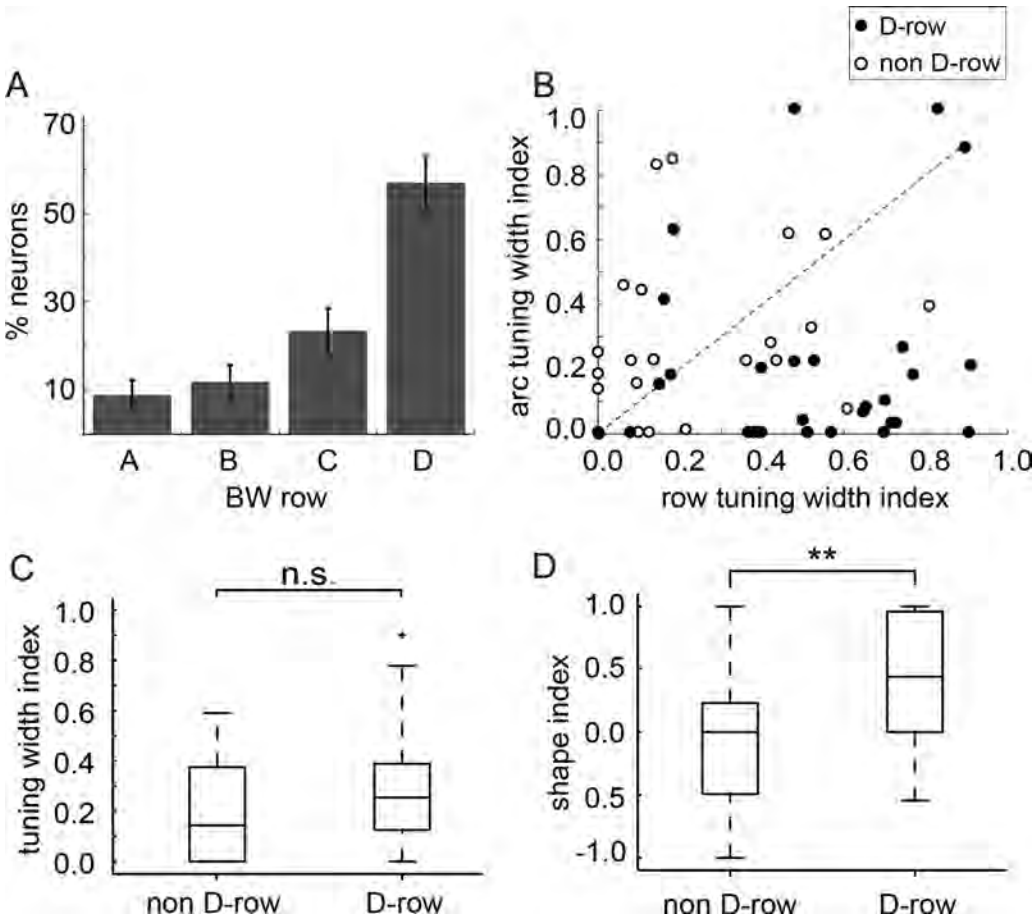

Figure 13. Tuning differences based on BW position. **A:** Distribution of BW positions for the data set of neurons in S1 that showed the greatest magnitude of response to the deflection of a mystacial whisker. Error bars show SE of the proportion. Our data set was dominated by neurons that had their BW in the D-row (57% D-row compared with 43% all non D-row whiskers). **B:** Scatterplot showing the relationship between the row tuning width index and arc tuning width index for individual neurons in S1. Neurons that had their BW in non D-rows (A–C rows) are denoted by open circles, and neurons that had their BW in the D-row are denoted by solid circles. Receptive fields for neurons with D-row BWs usually had higher row tuning width indices compared with arc tuning width indices, whereas the opposite was true for neurons with non D-row BWs, suggesting that the D-row group was more broadly tuned along the BW row and the non D-row group was more broadly tuned along the BW arc. **C:** Box plots comparing the tuning width indices of D-row and non D-row groups. Surrounding whiskers in both the D-row group and the non D-row group evoked a similar level of responsiveness relative to the BW ($P > 0.05$, Wilcoxon rank-sum test). **D:** Box plots comparing the shape indices of D-row and non D-row groups. The median shape index of the D-row group of neurons was significantly higher than that of non D-row neurons (**$P < 0.01$, Wilcoxon rank-sum test), indicating that, although the relative response magnitude to the surrounding whiskers is comparable in the D-row and non D-row groups as shown in C, the surround response is more skewed along the BW row rather than the BW arc for the D-row group of neurons.

it was often difficult to localize a single whisker within the receptive field that evoked the greatest magnitude of response because two or three neighboring whiskers evoked responses that were qualitatively similar.

Architecture of the S1 whisker region in *M. domestica*

Previous studies have examined the architectural structure of S1 (or, *area 3b*) in the short-tailed opossum with a variety of immunocytochemical and histological techniques (Huffman et al., 1999; Wong and Kaas, 2009). These studies were not able to demonstrate the presence of distinct barrel fields or barrel-like subdivisions in these animals, unlike rodents such as rats and mice or marsupials such as the brush-tailed possum, the striped possum, and the tammar wallaby (Woolsey et al., 1975; Waite et al., 1991; Weller, 1993; Huffman et al., 1999). In line with these previous studies, we found that cytochrome oxidase histochemistry, a technique that allows for the visualization of cortical barrel fields (Wong-Riley and Welt, 1980), failed to reveal barrel-like organization within the architectural boundaries of S1 (Fig. 4A–C). We further verified this lack of barrels by recording from the S1 whisker region in

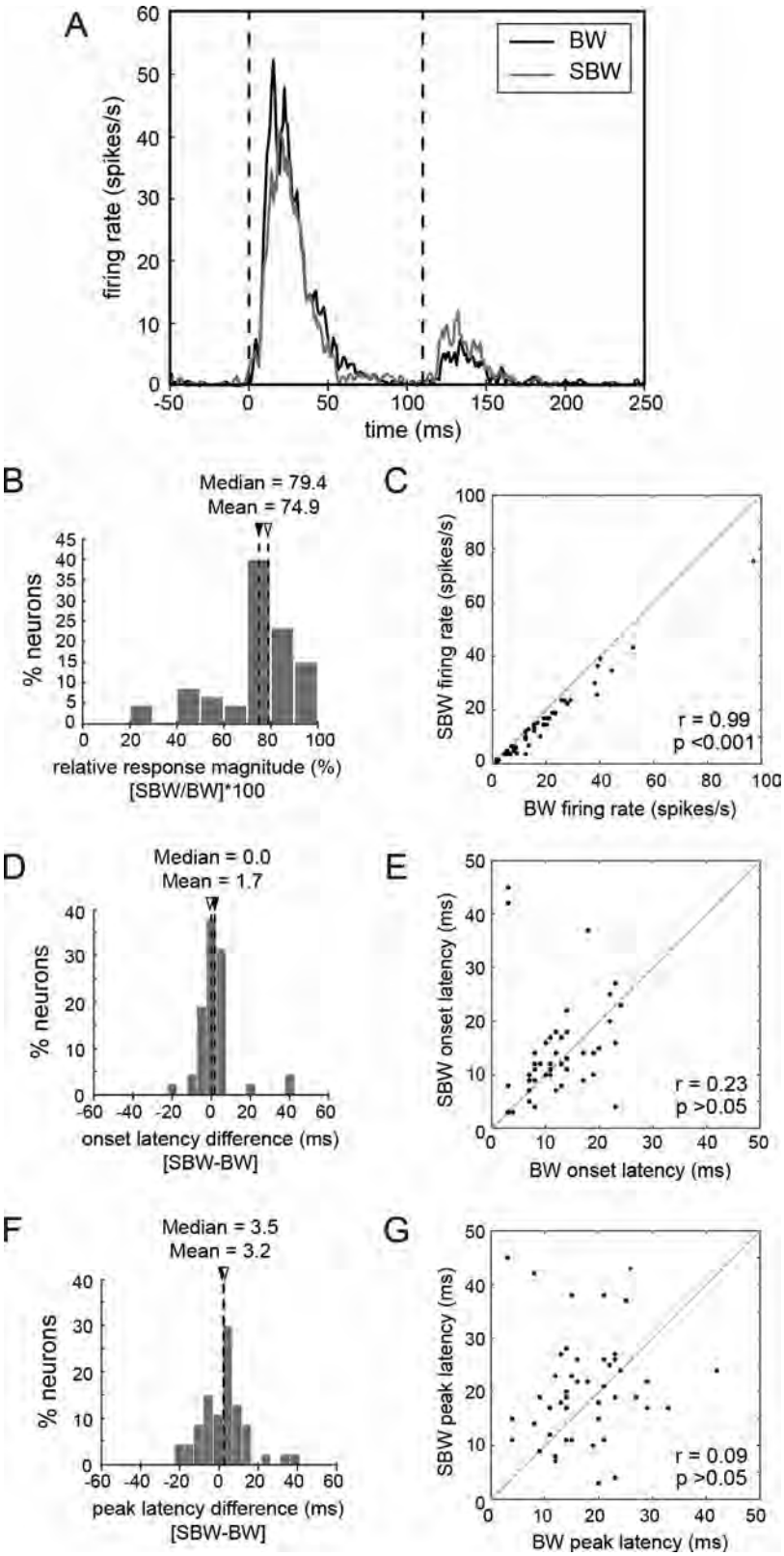
A
BW
SBW
firing rate (spikes/s)
time (ms)
B
Median = 79.4
Mean = 74.9
% neurons
relative response magnitude (%)
[SBW/BW]*100
C
SBW firing rate (spikes/s)
BW firing rate (spikes/s)
r = 0.99
p <0.001
D
Median = 0.0
Mean = 1.7
% neurons
onset latency difference (ms)
[SBW-BW]
E
SBW onset latency (ms)
BW onset latency (ms)
r = 0.23
p >0.05
F
Median = 3.5
Mean = 3.2
% neurons
peak latency difference (ms)
[SBW-BW]
G
SBW peak latency (ms)
BW peak latency (ms)
r = 0.09
p >0.05

Figure 14.

TABLE 2.
BW of Single Neurons Recorded per Penetration[1]

	Animals							
Penetrations	A	B	C	D	E	F	G	H
1	A2	A1	α	B1	A2	C3	D3	G6
2	A1, B3	B2	B3	C0	C3, C3, C3	C3, C3, D3		
3	α, B2	C4, C4, D5	B2, B2	C1	C2	C1, D2, D0		
4		C4, D4	B1	D3, D3, D2, D3	C2, D3	C0, D1		
5		D1, D1	C2	D2, D2	D3, D3	D3		
6			D2	D1, D1	D1, D1	D3		
7				D1	D1, D1, D3	D3		
8					D1, D2	D3		
9					D0	D2		
10						D1		
11						D1		
12						D1		
13						D0		

[1]Summary of the sampling of neurons that displayed a significant response to the deflection of at least one whisker (70/107). Each column lists the recording penetrations (1–13) for an individual animal (opossum A–H). In one animal (opossum I), no neurons were found to evoke a significant response as per our criteria (see Materials and Methods); therefore, this experiment does not appear here. For each penetration, the identity of the BW of each neuron analyzed per penetration is listed.

short-tailed opossums and by directly relating the locations of electrophysiological recording sites with the myeloarchitecture and cytoarchitecture of S1.

The relationship of electrophysiological recording sites to the architectural borders of S1 was determined by reconstructing tangential sections of the flattened cortex stained for myelin. Primary sensory areas, including S1, in short-tailed opossums were densely myelinated and darkly stained compared with surrounding cortical areas (Fig. 5A,B; Catania et al., 2000; Wong and Kaas, 2009; Dooley et al., 2013). Fluorescent probes were used to reconstruct the positions of electrode penetrations. Neurons that responded to the deflection of whiskers were located laterally in S1 (Fig. 5C) in correspondence with the location of the S1 whisker representation in somatotopic body maps of short-tailed opossums previously determined using microelectrode multiunit mapping techniques (Catania et al., 2000; Dooley et al., 2013). Myelin staining was uniformly dark in the region of the S1 whisker representation throughout all cortical layers, with no visible heterogeneities indicative of barrel-like organization. The relationship of electrophysiological recording sites to the laminar borders of S1 was determined by reconstructing coronal sections of the cortex stained in alternate series for parvalbumin (Fig. 6A) and Nissl substance (Fig. 6B). Layer IV of S1 stains darkly for parvalbumin-immunopositive terminals, along with several parvalbumin-immunopositive cell bodies (Wong and Kaas, 2009). Layer IV of S1 is also very well defined in Nissl-stained sections, appearing as a darkly stained band containing densely packed cell bodies (Karlen and

Figure 14. Temporal response characteristics of single neurons in S1. **A:** Population average PSTHs in response to the deflection of the BW (black line) and the SBW (gray line). Dashed lines indicate stimulus onset and offset. **B:** Distribution of the relative response magnitude to SBW deflection. Distribution for the entire data set is skewed toward the BW response (100%; mean 74.9% ± 2%, solid arrowhead; median 79.4% ± 3%, open arrowhead), indicating that, in most cases, the SBW evoked high-magnitude responses that were close to the value of the BW response. **C:** Scatterplot showing the relationship between the onset period firing rates following BW and SBW deflection; same data as in A,B. Although the deflection of the SBW evoked a firing rate close to the response evoked by the BW, the median difference in the magnitude of the responses to the BW and the SBW was significantly greater than 0 ($P < 0.001$, Wilcoxon signed-rank test). **D:** Distribution of the differences in the onset latencies of BW and SBW evoked responses. Distribution for the entire data set peaks at approximately 0 msec (mean 1.7 ± 1.4 msec, solid arrowhead; median 0.0 ± 1.7 msec, open arrowhead), suggesting that there is little difference in the onset latencies of the responses to the BW and the SBW. **E:** Scatterplot showing the relationship between the onset latencies of the neural responses following BW and SBW deflection; same data as in A,D. The median difference in the onset latencies of the responses to the BW and the SBW was not significantly different from 0 ($P > 0.05$, Wilcoxon signed-rank test). **F:** Distribution of the differences in the peak latencies of BW and SBW evoked responses. Distribution was slightly skewed toward positive values (mean 3.2 ± 1.7 msec, solid arrowhead; median 3.5 ± 2.1 msec, open arrowhead), suggesting that there was only a small trend, if any, for the BW peak latency to precede the SBW peak latency. **G:** Scatterplot showing the relationship between the peak latencies of the neural responses following BW and SBW deflection; same data as in A,F. The median difference in the peak latencies of the responses to the BW and the SBW was not significantly different from 0 ($P > 0.05$, Wilcoxon signed-rank test).

Krubitzer, 2007; Wong and Kaas, 2009). A microlesion used to mark the position of a recording site in the S1 whisker representation is indicated in Figure 6A–C. Cytoarchitectural parcellation into barrelfields or barrel-like subdivisions cannot be detected in the S1 whisker region with either parvalbumin or Nissl staining.

Quantitative measurement of receptive fields

When hand mapping indicated an evoked response to at least one whisker, receptive fields and response characteristics of the neuron were quantitatively measured with computer-controlled ramp–hold–return stimuli (Fig. 3A–D). Receptive fields were measured by recording the activity of single neurons in response to the deflection of individual whiskers. Typically, neurons responded maximally to the deflection of a single whisker (BW) but also responded with a lower magnitude to multiple surrounding whiskers. For all recorded neurons (n =107), responses to the stimulation of the BW were measured as well as responses to the stimulation of an additional 14–18 mystacial whiskers and 6–7 genal whiskers so that the spatial receptive field measurements were as complete as possible. Figures 7 and 8 show examples of the responses of neurons in S1 to the computer-controlled deflection of individual whiskers. In the first example, the neuron had its receptive field on the mystacial whiskers and responded with the highest magnitude to the deflection of the D0 whisker (Fig. 7A–C). In addition, deflection of two surrounding whiskers, D1 and D2, also evoked significant neural responses; the D1 response was 65.0% of the D0 response, and the D2 response was 44.5% of the D0 response. In the second example, the neuron had its receptive field on the genal whiskers and responded with the highest magnitude to the deflection of the G6 whisker (Fig. 8A–C), whereas deflection of four surrounding whiskers, G5, G4, G3, and G2, produced significant neural responses that were 90.5%, 76.2%, 42.9%, and 14.3%, respectively, of the G6 response. Except for the example shown in Figure 8, for which the receptive field was present on the genal whiskers, all remaining responsive neurons (n = 69 neurons) in our data set had their receptive fields on the mystacial whiskers.

Spontaneous and evoked activity

When deflections with amplitudes ranging from 0.1° to 2.0° were applied to the BWs of individual neurons, these neurons displayed monotonically increasing stimulus strength–response functions (Fig. 9A). Response magnitudes rapidly increase between 0.1° and 0.5° (mean 0.1 ± 0.1 spikes/stimulus at 0.1°, 1.3 ± 0.2 spikes/stimulus at 0.5°) and on average begin to saturate at amplitudes higher than 0.5° (mean 1.8 ± 0.2 spikes/stimulus at 2.0°). However, in some cases, response magnitudes continued to increase between 1.5° and 2.0° (the two highest amplitudes for which neural responses were measured). For receptive field analyses, 2.0° deflections were used in all cases to maximize the recorded evoked response while maintaining an amplitude of deflection for which there was no detectable mechanical stimulation of whiskers, fur, or skin adjacent to the whisker held in the piezoelectric device.

In our data set, 49% (52/107) of neurons displayed a significant evoked response following stimulus onset alone, 17% (18/107) of neurons displayed a significant evoked response following both stimulus onset and offset, and 0% (0/107) of neurons displayed a significant evoked response following stimulus offset alone (Fig. 9B). The spontaneous firing rate was low (mean 0.6 ± 0.2 spikes/sec; median 0.2 ± 0.3 spikes/sec). Onset period firing rates were significantly different from spontaneous firing rates (mean 13.3 ± 1.8 spikes/sec, two-sample *t*-test, $P < 0.001$; median 9.0 ± 2.3 spikes/sec, Wilcoxon rank-sum test, $P < 0.001$). Offset period firing rates were lower than onset period firing rates (mean 7.0 ± 2.3 spikes/sec, two-sample *t*-test, $P < 0.05$; median 3.1 ± 2.9 spikes/sec, Wilcoxon rank-sum test, $P < 0.05$) but significantly different from spontaneous firing rates (two-sample *t*-test, $P < 0.001$; Wilcoxon rank-sum test, $P < 0.001$; Fig. 9C). For the data included in receptive field analyses (onset-responsive neurons, n = 70), the distributions of onset-period firing rates and offset-period firing rates were significantly different both from the spontaneous firing rate distribution (Fig. 9D) and from each other (two-sample Kolmogorov-Smirnov test, $P < 0.001$ in all cases). Subsequent analyses were restricted to the neurons that evoked a significant onset response (data corresponding to the solid and shaded bars in Fig. 9B); receptive field properties of offset responses were not analyzed in the current study.

Receptive field size

To characterize the extent of the whisker array that elicited a response in individual neurons, receptive field size was measured as the number of whiskers that evoked a significant response above spontaneous activity and ranged in size from one to fourteen whiskers (Fig. 10A). Median receptive field size for the population of recorded S1 neurons was 3.0 whiskers (mean receptive field size = 3.7). Among all responsive neurons, 31% (22/70) responded only to a single BW, whereas

the remaining neurons also responded to the deflection of multiple neighboring whiskers in addition to the BW. Most responsive neurons (87%, 61/70) had a receptive field size of seven or fewer whiskers. In more than half the data set (64%, 45/70), two or more whiskers in the receptive field elicited a firing rate greater than 50% of the response evoked by the BW (Fig. 10B). However, the average first-order adjacent whisker response was ~25% of the BW response, suggesting that overall tuning was narrow (Fig. 10C). There was a further decrease in the response magnitude to <15% of the BW magnitude at the second-order adjacent whisker positions.

Spatial configuration of receptive fields

Receptive fields were visualized with contour plots (Fig. 11A–E). This analysis did not seek to acquire a depiction of the entire receptive field (which, as noted above, could include from one to fourteen whiskers) but rather to examine the spatial configuration of the receptive field at positions immediately surrounding the BW, with the assumption that the BW is the center of the receptive field (see Materials and Methods for further details). Most receptive fields were oval or round (80%, 56/70, based on 50% response level; Fig. 11A–C), but more irregular shapes (20%, 14/70; based on 50% response level; Fig. 11D,E) were also observed.

The mean receptive field for single neurons in the S1 whisker representation of short-tailed opossums was calculated by averaging the spatial receptive fields, consisting of the BW and eight immediately adjacent surrounding whiskers, across all neurons (Fig. 12A,B). The mean evoked response at all eight surrounding whisker positions was less than 50% of the BW response, with the highest mean evoked response of 39% ± 4% at the rostroventral position and the lowest mean evoked response of 15% ± 5% at the dorsal position. Because of the morphology of the short-tailed opossum whisker pad (Fig. 2A–D), surrounding whiskers were not present at all eight positions for all recorded units (see Materials and Methods for details). Therefore, the mean receptive field was also calculated separately for the neurons ($n = 7$) in which surrounding whiskers were present at all eight positions. Again, the mean surround whisker evoked response was less than 50% of the BW response at all eight positions, ranging from 1% ± 1% to 12% ± 9% (Fig. 12C,D).

A tuning width index was calculated for each neuron as the ratio of the mean responses evoked by surrounding whiskers at the immediately adjacent positions to the response evoked by the BW. Overall, receptive fields were narrowly tuned (mean tuning width index, 0.25 ± 0.03; median tuning width index, 0.24 ± 0.04; Fig. 12E). Tuning width index was significantly positively correlated ($r = 0.55$, $P < 0.05$) for pairs of units that were recorded within the same penetration. Although, on average, two or three whiskers in each receptive field evoked greater than 50% of the BW response (Fig. 10B), mean surround values at all eight immediate surround whisker positions was <50% of the BW response (Fig. 12A–D). The dominant surround whisker (second-best whisker; SBW) was not consistently located at any specific surround position. In the neurons that displayed a significant response to at least two whiskers ($n = 48/70$), the SBW and the BW could be located in the same row (52%, 25/48) or different rows (48%, 23/48). Also, the SBW could be located rostral to the BW (44%, 21/48), caudal to the BW (46%, 22/48), or in the same arc as the BW (10%, 5/48).

To assess the symmetry of tuning, a shape index was calculated for each neuron by measuring the tuning width index separately for in-row surrounding whiskers and in-arc surrounding whiskers and then computing a contrast index with those values (see Materials and Methods). Symmetrically tuned neurons, defined as those with a shape index between –0.2 and +0.2, made up 36% (25/70) of sites, whereas the remaining neurons displayed asymmetrical tuning, with the receptive field skewed along either the row or the arc. More neurons had strongly skewed receptive fields (shape index less than –0.6 or greater than +0.6) along the BW row (31%, 22/70) than the BW arc (11%, 8/70). Median shape index was 0.00 ± 0.09, whereas mean shape index was 0.20 ± 0.07, indicating that the average receptive field was symmetrical, with a slight trend toward broader row tuning in the population. Shape index exhibited a weak trend toward positive correlation between pairs of units from the same recording penetration ($r = 0.14$, $P > 0.05$).

Tuning differences based on BW position

We observed that a larger proportion of neurons in our data set responded maximally to whiskers located in the D-row of the mystacial pad (57%, 39/69) compared with all other rows combined (43%, 30/69; Fig. 13A). Although this could be due either to a sampling bias in the location of the recording sites in our experiments or to a true magnification of the representation of the D-row whiskers in S1, we were interested in testing whether there were any systematic differences in the tuning of neurons that had their BWs in the D-row compared with those neurons that had their BWs in the other three rows.

In general, the D-row group of neurons had row tuning width indices that were higher than their arc tuning width indices (Fig. 13B), whereas a trend in the opposite direction was seen for the non D-row group of

neurons. There was no significant difference in the tuning width indices of the two groups (two-tailed two-sample *t*-test, $P > 0.05$; Wilcoxon rank-sum test, $P > 0.05$; Fig. 13C), suggesting that the average response evoked by the surrounding whiskers relative to the BW was similar in both groups. However, shape index was significantly higher for the D-row group of neurons than for the non-D-row group of neurons (two-tailed two-sample *t*-test, $P < 0.001$; Wilcoxon rank-sum test, $P < 0.01$; Fig. 13D). This indicates asymmetric tuning in the D-row group of neurons, with the in-row surround whiskers evoking a higher firing rate than the in-arc surround whiskers, on average. In contrast, non D-row whiskers were more likely to be asymmetrical along both axes, with a bias toward being elongated along the arc.

Temporal response characteristics

We examined the temporal characteristics of single neurons in S1 in response to the deflection of the BW and the surrounding whiskers. S1 neurons responded to BW deflection at short latencies, with the earliest responses occurring at <10-msec (Fig. 14, Table 3). For the neurons that displayed a significant response to at least two whiskers (n = 48), we compared the temporal characteristics of the neural response to the deflection of the BW and the SBW by examining the population average PSTHs (Fig. 14A). The average population neural activity exhibited a similar time course in response to BW and SBW deflection. The onset component of the PSTHs also displays similar firing rates for both BW and SBW deflection. The distribution of response magnitudes of the SBW relative to the BW demonstrated that, in a majority of cases, the SBW evoked a response that was greater than 50% of the BW response (mean 74.9% ± 2%; median 79.4% ± 3%; Fig. 14B) However, paired comparisons of the firing rate during the onset period (0–75 msec) show that there was a significant difference between the response evoked by the BW and the response evoked by the SBW (two-tailed paired sample *t*-test, $P < 0.001$; Wilcoxon signed-rank test, $P < 0.001$; Fig. 14C). The offset component of the neural response displayed a trend toward higher average firing rates in response to SBW deflection compared with BW deflection.

We compared the latencies of the response to BW and SBW deflection for the onset response as well as for the peak of the response. Onset latency differences between BW and SBW responses were centered about zero (mean 1.7 ± 1.4 msec; median 0.0 ± 1.7 msec; Fig. 14D). Pairwise comparisons between BW and SBW onset latencies were not significantly different (two-tailed paired sample *t*-test, $P > 0.05$; Wilcoxon signed-

TABLE 3.
Summary of Neural Response Magnitudes and Latencies for BW and SBW Deflection

	Response magnitude (spikes/stimulus)				Onset latency (msec)				Peak latency (msec)			
	BW		SBW		BW		SBW		BW		SBW	
	Mean	Median	Mean	Median	Mean	Median	Mean	Median	Mean	Median	Mean	Median
10-msec ramp, n = 48	1.42 ± 0.18	1.17 ± 0.22	1.12 ± 0.15	0.94 ± 0.19	12.0 ± 0.88	11.5 ± 1.11	13.8 ± 1.32	12.0 ± 1.66	17.3 ± 1.12	15.5 ± 1.40	20.5 ± 1.42	19.0 ± 1.78
4-msec ramp, n = 16	1.41 ± 0.17	1.24 ± 0.21	1.20 ± 0.16	1.12 ± 0.21	9.84 ± 2.02	7.00 ± 2.53	11.4 ± 3.11	7.00 ± 3.89	17.5 ± 3.10	13.0 ± 3.89	18.0 ± 3.62	14.0 ± 4.54

rank test, $P > 0.05$; Fig. 14E). Thus, cortical neurons began to respond to either BW or SBW deflection at similar times following the stimulus. In comparison with onset latency differences, the distribution of peak latency differences between BW and SBW responses was shifted toward positive values (mean 3.2 $\pm$ 1.7 msec; median 3.5 $\pm$ 2.1 msec; Fig. 14F). However, pairwise comparisons between BW and SBW peak latencies were not significantly different (two-tailed paired sample *t*-test, $P > 0.05$; Wilcoxon signed-rank test, $P > 0.05$; Fig. 14G). These results suggest that neural responses evoked by BW and surround whisker deflection exhibit a very low level of temporal segregation, if any, in layer IV of short-tailed opossum S1.

For a subset of neurons (23/107), we measured BW and SBW response magnitudes and latencies for stimuli with 10-msec ramps as well as 4-msec ramps (see Materials and Methods). Summary data are listed in Table 3. For neurons that exhibited a significant response to the stimulation of at least two whiskers (n = 16), the parameters quantifying the relationship between SBW and BW responses (relative response magnitude, onset latency difference, peak latency difference) were not significantly different for 4-msec ramp stimuli compared with 10-msec ramp stimuli (two-tailed paired sample *t*-test, $P > 0.05$; Wilcoxon signed-rank test, $P > 0.05$, in all cases).

DISCUSSION

Numerous studies have used electrophysiological recording techniques to examine qualitatively the functional organization of the somatosensory cortex in a variety of mammals, including species of monotremes (Krubitzer et al., 1995), marsupials (Huffman et al., 1999; Catania et al., 2000; Frost et al., 2000; for review see Karlen and Krubitzer, 2007), and placentals (for review see Jones and Peters, 1990). These comparative studies have provided important insights into the evolution of cortical fields in mammals and the relationships between cortical organization and specializations in peripheral morphology and behavior. Different morphological features are specialized for tactile behavior in different mammalian species; examples include the bill of a platypus (Krubitzer et al., 1995), the nasal star of a star-nosed mole (Catania et al., 1993), the forepaw of a raccoon (Welker and Seidenstein, 1959), the incisors of a naked mole rat (Catania and Remple, 2002), the whiskers of a rat (Welker, 1971), and the hand of a primate (Nelson et al., 1980). In each of these cases, there is an expansion of the representation of the behaviorally relevant body surface within S1. The proportion of S1 dedicated to representing the whiskers in short-tailed opossums (~20%; Catania et al., 2000) is similar to that in rats (20%; Welker 1971), underscoring the importance of whiskers as a tactile sensory array in short-tailed opossums (*M. domestica*).

We characterized the spatial and temporal response properties of neurons in the S1 whisker representation of the short-tailed opossum. This is the first investigation of receptive fields and response properties of neurons in the whisker representation in an animal that naturally lacks histologically detectable barrels and septa in S1 but uses its whiskers in a manner similar to that of rats and mice. Additionally, this is the first study to quantify receptive field characteristics of neurons in the somatosensory cortex of a non-eutherian mammal.

This comparative analysis of receptive field organization can provide insights into critical features of cortical circuits in mammals that have emerged for the processing of distinct sensory inputs and for the facilitation of touch-mediated detection and discrimination with specialized sensory effector organs. We focused on characterizing responses of neurons in layer IV because this is the main thalamorecipient layer in mammalian sensory cortex, and the spatial and temporal aspects of receptive field organization can be expected to affect subsequent processing in other cortical layers of S1 as well as higher order cortical areas.

We first discuss our findings on receptive field sizes in opossum S1 whisker representation in comparison with other mammalian species. We then address anisotropies and whisker-specific differences that we observed in our data and compare these results with literature available on the barrel cortex of mice and rats. Finally, we address the differences in spatial and temporal processing in opossums compared with rats and mice as well as certain strains of mutant mice that exhibit a barrelless cytoarchitectural phenotype in S1 similar to that observed naturally in the short-tailed opossum.

Spatial convergence of whisker inputs

Receptive fields of single neurons in S1 whisker representation have been well defined in rats and mice (Armstrong-James and Fox, 1987; Armstrong-James et al., 1992; Petersen and Sakmann, 2001; Brecht and Sakmann, 2002, Quairiaux et al., 2007; Li et al., 2009). Because the sensory array in the whisker system consists of a punctate distribution of receptors associated with a grid-like layout of sinus hairs, we first quantified receptive field sizes in terms of the total number of whiskers that evoked a significant response in S1 neurons. Reported values of mean receptive field size in rats have ranged from 1.58 (under fentanyl anesthesia;

Simons and Carvell, 1989) to eight (under barbiturate anesthesia; Waite and Taylor, 1978) whiskers.

As noted by Fox and Woolsey (2008), these receptive field estimates likely were influenced by a number of factors, including type of anesthesia and anesthetic depth, behavioral state (arousal and attention levels), type of stimulus applied (single-whisker vs. multiwhisker stimuli, temporal dynamics of stimuli), method of neural response detection (qualitative vs. quantitative), and definition of the neural response (threshold used to discriminate spontaneous vs. driven neural activity). We used urethane anesthesia, which is now commonly used for acute neurophysiological recording in rodents because of the stability of the anesthesia that can be achieved (Niell and Stryker, 2008). Under these conditions, our estimate of the receptive field size (mean 3.7 whiskers; median 3.0 whiskers) was in agreement with receptive field sizes reported for layer IV neurons in urethane-anesthetized rats (mean 3.2 whiskers. Ito, 1985; 4.0 whiskers, Armstrong-James and Fox, 1987). Most neurons in short-tailed opossum S1 exhibited multiwhisker receptive fields, responding predominantly to a single BW but also displaying a lower magnitude response to the deflection of surrounding whiskers. Thirty-one percent of S1 neurons displayed single-whisker receptive fields, similar to the proportion in layer IV of rodent barrel cortex (31%, Ito, 1985; 29%, Fox et al., 2003).

To date, quantitative estimations of receptive field sizes of single neurons in S1 whisker representation have not been obtained in any studies of nonrodent species. However, qualitative assessments of receptive field size from studies that focused on other aspects of neuronal responses are available in a few other species of placental mammals, namely, rabbits, cats, and shrews.

In studies seeking to examine direction selectivity of the BW, receptive field sizes of inhibitory interneurons in layer IV of rabbit S1 were qualitatively assessed (55% of which were observed to have single-whisker receptive fields in awake rabbits; Swadlow 1989; Swadlow and Gusev 2002; Alonso et al., 2005). However, the mean tuning width of S1 neurons in the current study was closer to mean tuning width of regular-spiking excitatory neurons in mice (Gabernet et al., 2005), suggesting that our data set was dominated by excitatory neurons. Therefore, our data cannot be compared directly with available data from the rabbit barrel cortex. In S1 of cats, single neurons were observed to have multiwhisker receptive fields with a gradient-like organization (Schultz et al., 1976; Fomovskii, 1980). Thirty-nine percent of neurons in cat S1 responded to only a single whisker (qualitative assessment under barbiturate anesthesia; Schultz, 1976).

Receptive fields of multiunit activity combined across different lamina in S1 were reported in one study on the cortical organization in the Etruscan shrew (*Suncus etruscus*), a nocturnal, insectivorous tactile specialist that uses its whiskers to hunt prey (Anjum et al., 2006; Roth-Alpermann et al., 2010; Brecht et al., 2011; Naumann et al., 2012). The mean receptive field size in shrew S1, measured under urethane anesthesia, was 10 whiskers. This is much larger than receptive fields in S1 in rodents and short-tailed opossums with the same anesthetic; however, it is difficult to make direct comparisons with our data for two reasons. First, the shrew data are based on multiunit activity, which could lead to larger estimates of receptive field size; second, quantitatively assessed data were obtained only in one animal (although this estimate was reportedly consistent with hand-mapping data of multiunit whisker receptive fields obtained in additional experiments).

Receptive fields have been measured in S1 representations of a few other specialized touch systems in mammals, such as the nasal star in star-nosed moles and the hands of primates. Most receptive fields of single neurons in the S1 star representation were confined to a single star appendage (average RF size <1 mm^2; Sachdev and Catania, 2002). Similarly, in the S1 (area 3b) hand representation of rhesus macaque, single neuron receptive fields were mostly confined to a single digit (average RF size 14 mm^2; DiCarlo et al., 1998).

In all species examined to date, neurons in S1 whisker representation respond to the deflection of more than one whisker; that is, there is convergence of sensory inputs across multiple whiskers. However, the morphology of the sensory apparatus in the whisker system is very different from the nasal star (Sachdev and Catania, 2002) or the hand. An individual whisker deflection consists of a point-like stimulus on the sensory epithelium. In contrast, each appendage of the star and each digit of the primate hand has a large, continuous surface area that is covered by several touch receptors. Because of these differences in peripheral morphology, it is difficult to make direct comparisons of the spatial convergence of inputs in the whisker system with other specialized touch systems in mammals.

Asymmetries in spatial tuning of neurons

Prior reports of the spatial tuning of neurons in layer IV of barrel cortex in mice and rats have indicated mostly small, symmetrical receptive fields compared with neurons in other cortical layers (Chapin, 1986; Armstrong-James and Fox, 1987; Welker et al., 1993).

However, in these studies, asymmetry of tuning was not quantified for individual neurons; it was reported either qualitatively, or quantitatively from the mean receptive fields after averaging across all neurons. The mean receptive field for our data set (Fig. 12A,B) indicated a relative response magnitude of less than 50% of the BW response at all first-order adjacent whisker positions, similar to layer IV neurons in mice (Welker et al., 1993); however, a slight elongation of the receptive field along the row axis was observed (apparent in the contour plot; Fig. 12A). To examine the distribution of receptive field shapes across the data set, we quantified the tuning shape of receptive fields of neurons in S1 whisker representation in the short-tailed opossum using a continuous variable, the shape index (for further details see Materials and Methods). With this method, we found a substantial proportion of neurons with highly symmetric receptive fields (36%) in layer IV of S1, in line with previous studies. However, we also found that 40% of the neurons were highly asymmetrically tuned along either the row (31%) or the arc (11%), with a bias toward neurons more broadly tuned along the row.

This is in agreement with reports of anisotropic anatomical and functional organization in barrel cortex of mice and rats, which displays a bias toward integration of inputs from whiskers within the same row rather than those from different rows. S1 barrel columns corresponding to the same row of whiskers are more similar to each other in terms of neuronal numbers compared with barrel columns corresponding to whiskers in different rows (Meyer et al., 2013). In mice, barrel columns representing whiskers within the same row are more highly interconnected than those belonging to different rows (Bernardo et al., 1990). Voltage-sensitive dye imaging and electrophysiological recordings in barrel cortex of rats have demonstrated that single-whisker stimulation initially evokes responses in the barrel column corresponding to the stimulated whisker; however, the responses subsequently spread across the barrel cortex, with preferential activation of barrel columns within the same row (Armstrong-James and Fox, 1987; Lustig et al., 2013). Additionally, in rats, S1 barrels within the same row show higher levels of overlap of projection zones in other cortical areas (S2 and M1) compared with barrels representing different rows of whiskers (Hoffer et al., 2003).

Thus, a common feature of receptive field shape in the few species that have been studied is an elongation within a row of whiskers. Systematic biases toward asymmetries along any specific axes have not been found in the receptive fields for neurons located within the hand representation in rhesus macaques (DiCarlo et al., 1998). This might be due to differences in the morphology of the peripheral effectors involved. The hand has a continuous sheet of touch receptors and is used to manipulate objects, in addition to performing tactile detection and discrimination. In contrast, the whisker array, which consists of a punctate distribution of receptors associated with a grid of whiskers, is swept across objects in a stereotypic manner. Because whisking involves movements primarily along the rostrocaudal axis parallel to the whisker rows, whiskers within any given row are more likely to be stimulated together or in sequence, during the natural behavior of the animal. Therefore, integration of inputs from different whiskers within a row could facilitate the detection of the location and the tactile features of objects in the environment.

Whisker-specific differences in neuronal tuning

We found differences in the receptive field organization of neurons that were tuned to whiskers in the D-row, the ventralmost row of the mystacial array in short-tailed opossums, compared with neurons that were tuned to whiskers in rows A–C. Specifically, although there was no overall difference in tuning width, neurons with receptive fields on D-row whiskers were more broadly tuned along the row axis compared with the arc axis, resulting in more asymmetric receptive fields in these neurons. In contrast, neurons with receptive fields on whiskers in more dorsal rows had a tendency to be more broadly tuned along the arc axis rather than the row axis.

These results are consistent with reports of row-specific differences in the structural and functional organization of barrel cortex in rodents. Meyer and colleagues (2013) used high-resolution confocal imaging to reconstruct the cellular architecture of S1 barrel columns corresponding to different whiskers in the rat and found that there were significant differences in the structural organization of the barrel columns corresponding to different whiskers. The total number of neurons within each cortical barrel column increased from the most dorsal row of mystacial whiskers (A-row) to the most ventral row of mystacial whiskers (E-row). Additionally, there were whisker-specific differences in the laminar organization of the cortex in the barrel columns corresponding to the ventral rows of mystacial whiskers compared with those corresponding to the dorsal rows of whiskers. There is some evidence that these architectural differences among barrel columns corresponding to different whisker rows may be correlated with differences in functional organization. A

different study indicated that, in rat barrel cortex, layer IV neurons in E-row barrel columns displayed a stronger tendency to be preferentially activated by adjacent whiskers in the same row compared with neurons in the C-row and D-row barrel columns, which display less of a row preference (Armstrong-James and Fox, 1987).

In this study, neurons tuned to whiskers in the upper rows (A–C) displayed broader tuning along the arc, suggesting that there are high levels of connectivity among the representations of dorsal rows of whiskers with the ventral rows of whiskers. This is in agreement with studies of intracortical connections in mice that show preferential connectivity of the barrel columns of the small, dorsal whiskers with the large barrel columns of the E-row, in addition to being well connected with other small barrel columns.

Given the three-dimensional morphology of the whisker array in mammals with whisker-specific differences in the shape, size and orientation that depend on the position of the whisker in the array (Brecht et al., 1997; Towal et al., 2011), the fact that there are differences in the cortical organization corresponding to different whiskers is not surprising, although these differences have not been well explored. Ventral whisker rows are, in general, larger and more numerous than dorsal whisker rows, which could explain differences in neuronal numbers and cortical thickness of the associated barrel columns. Differences in tuning could be attributed to differences in the behavioral use of whiskers in the ventral rows compared with the dorsal rows because the ventral rows are closer to the ground during locomotion. For neurons that are tuned to whiskers in the ventralmost row (D-row in opossums, E-row in mice and rats), broader tuning along the row could potentially facilitate the detection of obstacles or inconsistencies in the animal's path or vibrations in the ground. The behavioral relevance of these ventral-row whiskers could lead to a magnification of their representation in the cortex, which could explain the overrepresentation of neurons tuned to the D-row in our data set. Overrepresentation of specific portions of specialized sensory effector arrays has been previously reported in the somatosensory system. For example, in the star-nosed mole, there is a magnification of the representation of the star in the S1 somatotopic map. Additionally, the 11th appendage of the star, which acts as a tactile fovea during foraging, is highly overrepresented within the S1 star representation (for review see Catania, 2012).

These studies, including the present work, show that whisker-specific differences in thalamic and cortical organization are counter to the notion that S1 cortex is composed of repeating, identical stereotypic units. Studies of receptive field organization and plasticity in mice and rats are frequently limited to neurons within specific barrel columns, usually C2 or D2, because the corresponding principal and adjacent whiskers can most easily be accessed for controlled stimulation. Although further work is required to link the whisker-specific differences in functional organization directly to differences in the structural organization of barrel columns, the existence of such whisker-specific differences should be considered in the interpretation of studies that are limited to individual barrel columns.

Temporal convergence of whisker inputs

The functional organization of barrel cortex in rats and mice is closely linked to its modular anatomy; there is a precise spatiotopic map of whiskers in layer IV of S1 in which neurons in each barrel respond primarily to a single BW (Welker, 1971; Armstrong-James and Fox, 1987). Neurons also respond to whiskers surrounding the best principal whisker, but there is a spatial and temporal segregation of the responses to the BW and the surrounding whiskers, with neurons having much longer latencies (5–30 msec delay; Armstrong-James and Fox, 1987; Armstrong-James and Callahan, 1991; Welker et al., 1993, 1996) when responding to stimulation of surround whiskers compared with stimulation of the BW, in addition to having much lower response magnitudes (20–30% of the BW response; Armstrong-James and Fox, 1987; Welker et al., 1996). The existence of these temporal differences in the responses of single neurons to different whiskers has led to the proposition that the timing of the neural response, in addition to the spike count, can encode information about the spatial location of a stimulus (Panzeri et al., 2001). In short-tailed opossums, we found that the SBW evoked high-magnitude responses (>70% BW response), with no significant delay relative to the BW. This suggests that timing differences in neural responses to the stimulation of different whiskers may not play a role in encoding stimulus location in short-tailed opossums. These interspecies differences in relative response latencies could be related to increased convergence of inputs at the subcortical or cortical levels in short-tailed opossums compared with mice and rats or could be due to differences in the connections of inhibitory circuits.

Neural response properties have previously been examined in a few different strains of mutant mice that exhibit a barrelless phenotype in S1 cortex. In adenylyl cyclase 1 loss-of-function mutant (*brl*) mice, there is an absence of barrel-like clustering of layer IV neurons as well as a lack of segregation of thalamocortical arbors in S1 (Welker et al., 1996; Abdel-Majid et al., 1998;

Gheorghita et al., 2006). In these mice, surround whiskers evoked high-magnitude responses (>50% BW response), with very little delay following the BW response (2.5 msec on average compared with an average of 13.5 msec in normal animals; Welker et al., 1996). Similarly, a lack of temporal segregation of best whisker and dominant surround whisker responses was reported in mGluR5 knockout mice, which lack layer IV cell clustering but retain thalamocortical arbor segregation in a portion of the S1 whisker representation (She et al., 2009). These findings, which are similar to our results in short-tailed opossums, suggest that discrete barrels may be part of an architecture that creates a latency difference in BW and surround whisker input. However, temporal segregation of BW and surround whisker responses was present in monoamine oxidase A knockout mutant (Tg8) mice, which lack both layer IV cell clusters and thalamocortical arbor segregation (Yang et al., 2001). Tg8 mice display normal whisker-related patterning at subcortical levels (Cases et al., 1996), unlike *brl* mice, which display more poorly defined barreloids in the thalamic ventrobasal nucleus compared with normal animals (Welker et al., 1996). This suggests that relative latency differences in BW and surround whisker input may not be directly related to modular organization at the level of the cortex but could be associated with segregation of whisker inputs at subcortical levels. Previous studies in short-tailed opossums (Olkowicz et al., 2008) have noted the absence of visible parcellation in the ventrobasal nucleus of the thalamus; parcellation in the trigeminal brainstem has not been examined to date. However, visualization of barreloids can require sectioning of the thalamus at angles that are oblique to standard cutting planes (Haidarliu and Ahissar, 2001). Furthermore, segmentation in both cortical and subcortical structures may be more clearly identified in juvenile brain tissue compared with adult brain tissue (Haidarliu and Ahissar, 2001; Catania et al., 2013). Therefore, to acquire a better understanding of parcellation of the whisker-to-cortex pathway in short-tailed opossums, a more thorough examination of cortical and subcortical structures must be conducted over the course of development. It is plausible that, in animals possessing a modular organization of barrel cortex, this type of architectural structure and the accompanying microcircuitry optimize tactile discrimination by enhancing spatiotemporal segregation of the neural response to different whisker inputs. If so, differences in the architectural structure of S1 may be reflective of the tactile capabilities of different species. However, it is possible that animals that naturally do not possess barrels in whisker cortex, rather than being functionally impaired, use different and, possibly, simpler circuits and information encoding strategies for whisker-mediated touch sensation. In this case, studying rodents in comparison with a phylogenetically distant species such as *M. domestica* could help us understand aspects of cortical processing that are shared across mammalian species.

Evolution of whisker-mediated somatosensation in mammals

The prevalence of whiskers among extant mammals and the similarities in their structure and function in phylogenetically distant taxa, rodents and marsupials, suggest that this is an evolutionarily old system. The early common ancestors of therian mammals (marsupials and placentals) were likely nocturnal (Gerkema et al., 2013) and, therefore, might have relied heavily on the use of their whiskers to perform functions such as exploration and navigation that would later be taken over by the visual system in diurnal mammals. Although many more comparative studies are required to formulate firm conclusions with respect to the cortical organization of the whisker system in these early mammals, a few common themes can be observed from the available data, providing insights into shared features of cortical processing in mammals. At the early stages of cortical somatosensory processing, there is a large proportion of small, symmetrical receptive fields that could be involved in performing fine tactile discriminations. However, most neurons in layer IV respond to the stimulation of multiple whiskers, indicating the convergence of excitatory inputs across whiskers. This allows for integration of information across sensory receptors and would thereby favor the detection of tactile stimuli in the environment. In whisker-mediated somatosensation, there is a preferential integration of inputs along the horizontal rows of whiskers, coincident with the caudorostral sweep of the whiskers during whisking. Furthermore, much as in other sensory systems, stimuli that impinge upon different portions of the sensory receptor array are represented differently in the cortex. In the whisker system, there appears to be an overrepresentation of the ventralmost row of mystacial whiskers, a row that contains the largest whiskers. This is combined with differences in neuronal tuning such that there is a higher level of rowwise convergence of inputs in neurons tuned to ventral whiskers in comparison with the neurons tuned to whiskers in dorsal rows. This is consistent with the ventral whisker rows being more likely to come into contact with obstacles or inconsistencies in the path of the animal.

Thus, the similarities in the peripheral morphology and use of the whisker system in rodents and

marsupials are accompanied by a number of similarities in sensory processing of whisker inputs at the level of the cortex. These similarities are likely reflective of somatosensory neural circuits that emerged early in the course of mammalian evolution. The possession of a new tactile sensory specialization in the form of the whisker system would have conferred an adaptive advantage for a nocturnal life style and, therefore, played an important role in the survival of early, ancestral mammals.

ACKNOWLEDGMENTS

The authors are grateful to Drs. Daniel E. Feldman and Gregg H. Recanzone for many helpful discussions and for comments on a draft of the manuscript; Cynthia Weller, Rebecca Hao, and Dr. Brian Trainor for providing expertise and resources for Western blot analysis; Dr. Mary Baldwin for histological assistance and helpful suggestions with respect to this article; Drs. Dylan Cooke, James Dooley, and Adam Goldring for critically reading the article; Dr. Jeffrey Johnson for programming assistance; Dr. Cindy Clayton for animal care; and Adam Gordon, Raquel Valdes, and Krisha Yadav-Rajan for experimental assistance.

CONFLICT OF INTEREST STATEMENT

The authors declare that there are no identified conflicts of interest in relation to the current study.

ROLE OF AUTHORS

All authors had full access to all the data in the study and take responsibility for the integrity of the data and the accuracy of the data analysis. Study concept and design: DLR, LAK. Acquisition of data: DLR. Analysis and interpretation of data: DLR, LAK. Drafting of the manuscript: DLR, LAK. Critical revision of the article for important intellectual content: DLR, LAK. Statistical analysis: DLR. Obtained funding: DLR, LAK. Study supervision: LAK.

LITERATURE CITED

Abdel-Majid RM, Leong WL, Schalkwyk LC, Smallman DS, Wong ST, Storm DR, Fine A, Dobson MJ, Guernsey DL, Neumann PE. 1998. Loss of adenylyl cyclase I activity disrupts patterning of mouse somatosensory cortex. Nat Genet 19:289–291.

Ahl AS. 1986. The role of vibrissae in behavior: a status review. Vet Res Commun 10:245–268.

Alonso JM, Swadlow HA. 2005. Thalamocortical specificity and the synthesis of sensory cortical receptive fields. J Neurophysiol 94:26–32.

Anjum F, Turni H, Mulder PG, van der Burg J, Brecht M. 2006. Tactile guidance of prey capture in Etruscan shrews. Proc Natl Acad Sci U S A 103:16544–16549.

Armstrong-James M, Callahan CA. 1991. Thalamocortical processing of vibrissal information in the rat. II. Spatiotemporal convergence in the thalamic ventroposterior medial nucleus (VPm) and its relevance to generation of receptive fields of S1 cortical "barrel" neurones. J Comp Neurol 303:211–224.

Armstrong-James M, Fox K. 1987. Spatiotemporal convergence and divergence in the rat S1 "barrel" cortex. J Comp Neurol 263:265–281.

Armstrong-James M, Fox K, Das-Gupta A. 1992. Flow of excitation within rat barrel cortex on striking a single vibrissa. J Neurophysiol 68:1345–1358.

Bernardo KL, McCasland JS, Woolsey TA, Strominger RN. 1990. Local intra- and interlaminar connections in mouse barrel cortex. J Comp Neurol 291:231–255.

Bobrov E, Wolfe J, Rao RP, Brecht M. 2014. The representation of social facial touch in rat barrel cortex. Curr Biol 24:109–115.

Brecht M. 2007. Barrel cortex and whisker-mediated behaviors. Curr Opin Neurobiol 17:408–416.

Brecht M, Sakmann B. 2002. Dynamic representation of whisker deflection by synaptic potentials in spiny stellate and pyramidal cells in the barrels and septa of layer 4 rat somatosensory cortex. J Physiol 543:49–70.

Brecht M, Preilowski B, Merzenich MM. 1997. Functional architecture of the mystacial vibrissae. Behav Brain Res 84:81–97.

Brecht M, Roth A, Sakmann B. 2003. Dynamic receptive fields of reconstructed pyramidal cells in layers 3 and 2 of rat somatosensory barrel cortex. J Physiol 553:243–265.

Brecht M, Naumann R, Anjum F, Wolfe J, Munz M, Mende C, Roth-Alpermann C. 2011. The neurobiology of Etruscan shrew active touch. Philos Trans R Soc Lond B Biol Sci 366:3026–3036.

Cases O, Vitalis T, Seif I, De Maeyer E, Sotelo C, Gaspar P. 1996. Lack of barrels in the somatosensory cortex of monoamine oxidase A-deficient mice: role of a serotonin excess during the critical period. Neuron 16:297–307.

Catania KC. 2012. Evolution of brains and behavior for optimal foraging: a tale of two predators. Proc Natl Acad Sci U S A 109(Suppl 1):10701–10708.

Catania KC, Remple MS. 2002. Somatosensory cortex dominated by the representation of teeth in the naked mole-rat brain. Proc Natl Acad Sci U S A 99:5692–5697.

Catania KC, Northcutt RG, Kaas JH, Beck PD. 1993. Nose stars and brain stripes. Nature 364:493.

Catania KC, Jain N, Franca JG, Volchan E, Kaas JH. 2000. The organization of somatosensory cortex in the short-tailed opossum (*Monodelphis domestica*). Somatosens Mot Res 17:39–51.

Catania KC, Catania EH, Sawyer EK, Leitch DB. 2013. Barrelettes without barrels in the American water shrew. PLoS One 8:e65975.

Chapin JK. 1986. Laminar differences in sizes, shapes, and response profiles of cutaneous receptive fields in the rat SI cortex. Exp Brain Res 62:549–559.

Diamond ME, von Heimendahl M, Knutsen PM, Kleinfeld D, Ahissar E. 2008. "Where" and "what" in the whisker sensorimotor system. Nat Rev Neurosci 9:601–612.

DiCarlo JJ, Johnson KO, Hsiao SS. 1998. Structure of receptive fields in area 3b of primary somatosensory cortex in the alert monkey. J Neurosci 18:2626–2645.

Dooley JC, Franca JG, Seelke AM, Cooke DF, Krubitzer LA. 2013. A connection to the past: *Monodelphis domestica* provides insight into the organization and connectivity of the brains of early mammals. J Comp Neurol 521:3877–3897.

Feldmeyer D, Brecht M, Helmchen F, Petersen CC, Poulet JF, Staiger JF, Luhmann HJ, Schwarz C. 2013. Barrel cortex function. Prog Neurobiol 103:3–27.

Fomovskii BI. 1980. Somatosensory cortical unit responses to stimulation of the vibrissae in cats. Neurophysiology 12: 85–90.

Fox K, Woolsey T. 2008. Barrel cortex: Cambridge: Cambridge University Press.

Fox K, Wright N, Wallace H, Glazewski S. 2003. The origin of cortical surround receptive fields studied in the barrel cortex. J Neurosci 23:8380–8391.

Frost SB, Milliken GW, Plautz EJ, Masterton RB, Nudo RJ. 2000. Somatosensory and motor representations in cerebral cortex of a primitive mammal (*Monodelphis domestica*): a window into the early evolution of sensorimotor cortex. J Comp Neurol 421:29–51.

Gabernet L, Jadhav SP, Feldman DE, Carandini M, Scanziani M. 2005. Somatosensory integration controlled by dynamic thalamocortical feedforward inhibition. Neuron 48:315–327.

Gallyas F. 1979. Silver staining of myelin by means of physical development. Neurol Res 1:203–209.

Gerkema MP, Davies WIL, Foster RG, Menaker M, Hut RA. 2013. The nocturnal bottleneck and the evolution of activity patterns in mammals. Proc Biol Sci 280: 20130508.

Gheorghita F, Kraftsik R, Dubois R, Welker E. 2006. Structural basis for map formation in the thalamocortical pathway of the barrelless mouse. J Neurosci 26:10057–10067.

Grant RA, Haidarliu S, Kennerley NJ, Prescott TJ. 2013. The evolution of active vibrissal sensing in mammals: evidence from vibrissal musculature and function in the marsupial opossum *Monodelphis domestica*. J Exp Biol 216:3483–3494.

Haidarliu S, Ahissar E. 2001. Size gradients of barreloids in the rat thalamus. J Comp Neurol 429:372–387.

Heesy CP, Hall MI. 2010. The nocturnal bottleneck and the evolution of mammalian vision. Brain Behav Evol 75:195–203.

Hoffer ZS, Hoover JE, Alloway KD. 2003. Sensorimotor corticocortical projections from rat barrel cortex have an anisotropic organization that facilitates integration of inputs from whiskers in the same row. J Comp Neurol 466:525–544.

Huber E. 1930a. Evolution of facial musculature and cutaneous field of trigeminus. Part I. Q Rev Biol 5:133–188.

Huber E. 1930b. Evolution of facial musculature and cutaneous field of trigeminus. Part II. Q Rev Biol 5:389–437.

Huffman KJ, Nelson J, Clarey J, Krubitzer L. 1999. Organization of somatosensory cortex in three species of marsupials, *Dasyurus hallucatus*, *Dactylopsila trivirgata*, and *Monodelphis domestica*: neural correlates of morphological specializations. J Comp Neurol 403:5–32.

Ito M. 1985. Processing of vibrissa sensory information within the rat neocortex. J Neurophysiol 54:479–490.

Jones EG, Peters A. 2012. Cerebral cortex: comparative structure and evolution of cerebral cortex. New York: Springer.

Karlen SJ, Krubitzer L. 2007. The functional and anatomical organization of marsupial neocortex: evidence for parallel evolution across mammals. Prog Neurobiol 82:122–141.

Kemp TS. 2005. The origin and evolution of mammals. Oxford: Oxford University Press.

Kim U, Ebner FF. 1999. Barrels and septa: separate circuits in rat barrels field cortex. J Comp Neurol 408:489–505.

Koralek KA, Jensen KF, Killackey HP. 1988. Evidence for two complementary patterns of thalamic input to the rat somatosensory cortex. Brain Res 463:346–351.

Krubitzer L, Manger P, Pettigrew J, Calford M. 1995. Organization of somatosensory cortex in monotremes: in search of the prototypical plan. J Comp Neurol 351:261–306.

Lee KJ, Woolsey TA. 1975. A proportional relationship between peripheral innervation density and cortical neuron number in the somatosensory system of the mouse. Brain Res 99:349–353.

Li L, Bender KJ, Drew PJ, Jadhav SP, Sylwestrak E, Feldman DE. 2009. Endocannabinoid signaling is required for development and critical period plasticity of the whisker map in somatosensory cortex. Neuron 64:537–549.

Loo SK, Halata Z. 1991. Innervation of hairs in the facial skin of marsupial mammals. J Anat 174:207–219.

Lu SM, Lin RC. 1993. Thalamic afferents of the rat barrel cortex: a light- and electron-microscopic study using *Phaseolus vulgaris* leucoagglutinin as an anterograde tracer. Somatosens Mot Res 10:1–16.

Lustig BR, Friedman RM, Winberry JE, Ebner FF, Roe AW. 2013. Voltage-sensitive dye imaging reveals shifting spatiotemporal spread of whisker-induced activity in rat barrel cortex. J Neurophysiol 109:2382–2392.

Lyne AG. 1959. The systematic and adaptive significance of the vibrissae in the *Marsupialia*. Proc Zool Soc Lond 133: 79–133.

Meredith RW, Janecka JE, Gatesy J, Ryder OA, Fisher CA, Teeling EC, Goodbla A, Eizirik E, Simao TL, Stadler T, Rabosky DL, Honeycutt RL, Flynn JJ, Ingram CM, Steiner C, Williams TL, Robinson TJ, Burk-Herrick A, Westerman M, Ayoub NA, Springer MS, Murphy WJ. 2011. Impacts of the cretaceous terrestrial revolution and KPg extinction on mammal diversification. Science 334:521–524.

Meyer HS, Egger R, Guest JM, Foerster R, Reissl S, Oberlaender M. 2013. Cellular organization of cortical barrel columns is whisker specific. Proc Natl Acad Sci U S A 110:19113–19118.

Mitchinson B, Grant RA, Arkley K, Rankov V, Perkon I, Prescott TJ. 2011. Active vibrissal sensing in rodents and marsupials. Philos Trans R Soc Lond B Biol Sci 366: 3037–3048.

Naumann RK, Anjum F, Roth-Alpermann C, Brecht M. 2012. Cytoarchitecture, areas, and neuron numbers of the Etruscan shrew cortex. J Comp Neurol 520:2512–2530.

Nelson RJ, Sur M, Felleman DJ, Kaas JH. 1980. Representations of the body surface in postcentral parietal cortex of *Macaca fascicularis*. J Comp Neurol 192:611–643.

Niell CM, Stryker MP. 2008. Highly selective receptive fields in mouse visual cortex. J Neurosci 28:7520–7536.

Nomura S, Itoh K, Sugimoto T, Yasui Y, Kamiya H, Mizuno N. 1986. Mystacial vibrissae representation within the trigeminal sensory nuclei of the cat. J Comp Neurol 253: 121–133.

O'Leary MA, Bloch JI, Flynn JJ, Gaudin TJ, Giallombardo A, Giannini NP, Goldberg SL, Kraatz BP, Luo ZX, Meng J, Ni X, Novacek MJ, Perini FA, Randall ZS, Rougier GW, Sargis EJ, Silcox MT, Simmons NB, Spaulding M, Velazco PM, Weksler M, Wible JR, Cirranello AL. 2013. The placental mammal ancestor and the post-K-Pg radiation of placentals. Science 339:662–667.

Olkowicz S, Turlejski K, Bartkowska K, Wielkopolska E, Djavadian RL. 2008. Thalamic nuclei in the opossum *Monodelphis domestica*. J Chem Neuroanat 36:85–97.

Panzeri S, Petersen RS, Schultz SR, Lebedev M, Diamond ME. 2001. The role of spike timing in the coding of stimulus location in rat somatosensory cortex. Neuron 29:769–777.

Patrizi G, Munger BL. 1966. The ultrastructure and innervation of rat vibrissae. J Comp Neurol 126:423–435.

Petersen CC, Sakmann B. 2001. Functionally independent columns of rat somatosensory barrel cortex revealed with voltage-sensitive dye imaging. J Neurosci 21:8435–8446.

Pocock R. 1914. 48. On the facial vibrissæ of mammalian. Proc Zool Soc Lond. Wiley Online Library. http://onlinelibrary.wiley.com/doi/10.1111/j.1469-7998.1914.tb07067.x/full

Quairiaux C, Armstrong-James M, Welker E. 2007. Modified sensory processing in the barrel cortex of the adult

mouse after chronic whisker stimulation. J Neurophysiol 97:2130–2147.
Roskov Y, Abucay L, Orrell T, Nicolson D, Kunze T, Culham A, Bailly N, Kirk P, Bourgoin T, DeWalt RE, Decock W, De Wever A, editors. 2015. Species 2000 & ITIS catalogue of life, 2015 annual checklist. Digital resource at www.catalogueoflife.org/annual-checklist/2015
Roth-Alpermann C, Anjum F, Naumann R, Brecht M. 2010. Cortical organization in the Etruscan shrew (*Suncus etruscus*). J Neurophysiol 104:2389–2406.
Sachdev RN, Catania KC. 2002. Receptive fields and response properties of neurons in the star-nosed mole's somatosensory fovea. J Neurophysiol 87:2602–2611.
Sarko DK, Rice FL, Reep RL. 2011. Mammalian tactile hair: divergence from a limited distribution. Ann N Y Acad Sci 1225:90–100.
Schultz W, Galbraith GC, Gottschaldt KM, Creutzfeldt OD. 1976. A comparison of primary afferent and cortical neurone activity coding sinus hair movements in the cat. Exp Brain Res 24:365–381.
She WC, Quairiaux C, Albright MJ, Wang YC, Sanchez DE, Chang PS, Welker E, Lu HC. 2009. Roles of mGluR5 in synaptic function and plasticity of the mouse thalamocortical pathway. Eur J Neurosci 29:1379–1396.
Simons DJ. 1978. Response properties of vibrissa units in rat SI somatosensory neocortex. J Neurophysiol 41:798–820.
Simons DJ, Carvell GE. 1989. Thalamocortical response transformation in the rat vibrissa/barrel system. J Neurophysiol 61:311–330.
Sofroniew NJ, Cohen JD, Lee AK, Svoboda K. 2014. Natural whisker-guided behavior by head-fixed mice in tactile virtual reality. J Neurosci 34:9537–9550.
Sofroniew NJ, Svoboda K. 2015. Whisking. Curr Biol 25:R137–140.
Swadlow HA. 1989. Efferent neurons and suspected interneurons in S-1 vibrissa cortex of the awake rabbit: receptive fields and axonal properties. J Neurophysiol 62:288–308.
Swadlow HA, Gusev AG. 2002. Receptive-field construction in cortical inhibitory interneurons. Nat Neurosci 5:403–404.
Towal RB, Quist BW, Gopal V, Solomon JH, Hartmann MJ. 2011. The morphology of the rat vibrissal array: a model for quantifying spatiotemporal patterns of whisker–object contact. PLoS Comput Biol 7:e1001120.
Waite PM, Taylor PK. 1978. Removal of whiskers in young rats causes functional changes in cerebral cortex. Nature 274:600–602.
Waite PM, Marotte LR, Mark RF. 1991. Development of whisker representation in the cortex of the tammar wallaby *Macropus eugenii*. Brain Res Dev Brain Res 58:35–41.
Welker C. 1971. Microelectrode delineation of fine grain somatotopic organization of SmI cerebral neocortex in albino rat. Brain Res 26:259–275.
Welker C. 1976. Receptive fields of barrels in the somatosensory neocortex of the rat. J Comp Neurol 166:173–189.
Welker E, Van der Loos H. 1986. Quantitative correlation between barrel-field size and the sensory innervation of the whiskerpad: a comparative study in six strains of mice bred for different patterns of mystacial vibrissae. J Neurosci 6:3355–3373.
Welker E, Armstrong-James M, Van der Loos H, Kraftsik R. 1993. The mode of activation of a barrel column: response properties of single units in the somatosensory cortex of the mouse upon whisker deflection. Eur J Neurosci 5:691–712.
Welker E, Armstrong-James M, Bronchti G, Ourednik W, Gheorghita-Baechler F, Dubois R, Guernsey DL, Van der Loos H, Neumann PE. 1996. Altered sensory processing in the somatosensory cortex of the mouse mutant barrelless. Science 271:1864–1867.
Welker WI, Seidenstein S. 1959. Somatic sensory representation in the cerebral cortex of the raccoon (*Procyon lotor*). J Comp Neurol 111:469–501.
Weller WL. 1993. SmI cortical barrels in an Australian marsupial, *Trichosurus vulpecula* (brush-tailed possum): structural organization, patterned distribution, and somatotopic relationships. J Comp Neurol 337:471–492.
Wong P, Kaas JH. 2009. An architectonic study of the neocortex of the short-tailed opossum (*Monodelphis domestica*). Brain Behav Evol 73:206–228.
Wong-Riley MTT. 1989. Cytochrome oxidase: an endogenous metabolic marker for neuronal activity. Trends Neurosci 12:94–101.
Wong-Riley MT, Welt C. 1980. Histochemical changes in cytochrome oxidase of cortical barrels after vibrissal removal in neonatal and adult mice. Proc Natl Acad Sci U S A 77:2333–2337.
Woolsey TA, Van der Loos H. 1970. The structural organization of layer IV in the somatosensory region (SI) of mouse cerebral cortex. The description of a cortical field composed of discrete cytoarchitectonic units. Brain Res 17:205–242.
Woolsey TA, Welker C, Schwartz RH. 1975. Comparative anatomical studies of the SmL face cortex with special reference to the occurrence of "barrels" in layer IV. J Comp Neurol 164:79–94.
Yang Z, Seif I, Armstrong-James M. 2001. Differences in somatosensory processing in S1 barrel cortex between normal and monoamine oxidase A knockout (Tg8) adult mice. Cereb Cortex 11:26–36.